Border-collision bifurcations in $\mathbb{R}^N$.

D.J.W. Simpson

Institute of Fundamental Sciences
Massey University
Palmerston North
New Zealand

August 4, 2015

Abstract

For piecewise-smooth maps, new dynamics can be created by varying parameters such that a fixed point collides with a surface on which the map is nonsmooth. If the map is continuous and piecewise-linear to leading order, this is referred to as a border-collision bifurcation. A lack of differentiability allows for substantial complexity and a wide variety of invariant sets can be created in border-collision bifurcations, such as invariant circles and chaotic sets, and several attractors may be created simultaneously. Yet many calculations that would be intractable for smooth nonlinear maps can be performed exactly for piecewise-linear maps and in recent years several new results have been obtained for border-collision bifurcations. This paper reviews border-collision bifurcations with a general emphasis on results that apply to maps of any number of dimensions. The paper covers applications, the border-collision normal form, basic properties and dynamics such as fixed points, periodic solutions and mode-locking regions, and more complex phenomena such as multistability, multi-dimensional attractors, attractors at infinity, homoclinic bifurcations and unfoldings of codimension-two scenarios.

1 Introduction

PWS (piecewise-smooth) systems are increasingly being used as mathematical models in diverse areas. A *PWS map* on $\mathcal{M} \subset \mathbb{R}^N$ is a discrete-time evolution rule

$$x_{i+1} = f^J(x_i) \,, \qquad x_i \in \mathcal{M}_J \,, \tag{1.1}$$

where the regions $\mathcal{M}_J$ form a partition of $\mathcal{M}$, and each $f^J : \mathcal{M}_J \to \mathcal{M}$ is a smooth function. Boundaries of the $\mathcal{M}_J$, termed *switching manifolds*, are assumed to be PWS codimension-one surfaces. Maps of the form (1.1) arise as return maps of nonsmooth systems of differential equations. In this context, applications include mechanical systems with impacts or friction [16, 24, 26, 122, 193], power electronics and relay control [20, 108, 201], and more recently

ecological systems involving quotas or switching of species between different habitats or food sources [4, 45, 154, 185]. PWS maps are also used to model discrete-time phenomena involving a switch, choice or threshold, such as economics systems involving non-negativity conditions, decisions or optimisation [28, 105, 120, 158]. Other applications of (1.1) include bursting in neurons [43, 162], Chua's circuit [133], and game theory [151]. Maps that are continuous and PWL (piecewise-linear), such as the tent map and the Lozi map [127, 142] (a PWL version of the Hénon map), are used throughout dynamical systems and are particularly relevant to this paper.

Interactions between invariant sets and switching manifolds of (1.1) give rise to *discontinuity-induced bifurcations* [52]. The simplest type of discontinuity-induced bifurcation for (1.1) corresponds to the collision of a fixed point with a smooth part of a switching manifold. Generically this involves two functional components of (1.1), call them f^L and f^R (for "left" and "right"). Dynamics near the bifurcation are described by the local representation

$$x_{i+1} = \begin{cases} f^L(x_i) \,, & h(x_i) < 0 \\ f^R(x_i) \,, & h(x_i) \geq 0 \end{cases} \,, \tag{1.2}$$

where h is a smooth function specifying the switching manifold. At the bifurcation one of the half-maps (f^L and f^R) has a fixed point on the switching manifold ($h = 0$).

Many essential features of the bifurcation are determined by the local properties of (1.2) and there are a handful of distinct scenarios that commonly arise. For instance, (1.2) may be discontinuous. Discontinuous maps are frequently used to model excitable systems [39, 89], and circuit systems [68, 106]. Alternatively, (1.2) may be continuous but involve a square-root singularity in either f^L or f^R. This scenario arises naturally in grazing bifurcations of vibro-impacting systems (the singularity results from a quadratic tangency between a periodic orbit and a switching manifold) [51, 143, 145, 146]. In any case, the bifurcation is a type of *border-collision*, but the term *border-collision bifurcation* is usually reversed for the situation that (1.2) is continuous and PWL to leading order. This definition is adopted in this paper. The dynamics of discontinuous maps are described in [12, 13, 66, 103, 159], maps with a square-root singularity in [10, 34, 65, 77, 147], and other maps in [52].

It is instructive to compare BCBs (border-collision bifurcations) with classical bifurcations of smooth maps, to which it is assumed the reader is familiar. For definiteness, let us consider period-doubling (or flip) bifurcations. BCBs and period-doubling bifurcations are both local, codimension-one bifurcations of fixed points, with the following key differences:

i) For a period-doubling bifurcation, as parameters are varied a stability multiplier of the fixed point continuously passes through the value -1. For a BCB, since the map is continuous but non-differentiable, the stability multipliers of the fixed point change discontinuously at the bifurcation, and one or more multipliers can "jump" across the unit circle.

ii) Dynamics related to a period-doubling bifurcation are fully described by the restriction of the map to a two-dimensional extended centre manifold. For a typical BCB, there is no centre manifold. Indeed for PWS systems in general a lack global differentiability inhibits the construction of a centre manifold and dimension reduction.

iii) At a period-doubling bifurcation a period-2 solution is created, and we can determine the side of the bifurcation for which the period-doubled solution exists via straight-forward

direct calculations. At a BCB, a seemingly inexhaustible array of invariant sets can be created. Simple calculations suffice to identify fixed points and period-2 solutions. Other dynamics can be determined numerically or with more sophisticated methods, as discussed in later sections.

iv) As we move away from a period-doubling bifurcation, the period-2 solution grows at a rate asymptotically proportional to the square root of the parameter change. In contrast, any bounded invariant set created in a BCB grows linearly, to leading order, with parameter change.

Such differences can be identified qualitatively from the measurements of a physical system, lending support, or not, to the use of a mathematical model that is nonsmooth. For example, in [199, 200] it is found that the linear scaling laws associated with a BCB provide a better fit to experimental data for the action potential duration of cardiac cells than those for a period-doubling bifurcation, suggesting that a nonsmooth (or highly nonlinear) model is more appropriate than a smooth model.

The term BCB was coined in the pioneering 1992 paper of Nusse and Yorke [148]. The paper describes various fundamental aspects of BCBs in two dimensions and was motivated by novel dynamics in economics models [104, 105]. Some study of BCBs had been performed earlier. In particular, in the Russian literature at least as early the 1960's, BCBs were studied and referred to as C-bifurcations, after the word сшивать, which means to "sew" (or "stitch"). The behaviour of fixed points and period-2 solutions near BCBs was studied in [27] and [69] respectively. In [70], Feigin determined an efficient and practical method for identifying fixed points and period-2 solutions based on the computation of eigenvalues.

Grazing bifurcations of nonsmooth systems of differential equations originally provided much motivation for BCBs, but in [51] it was shown that *regular grazing bifurcations* involve a square-root singularity, and are therefore not BCBs. However, the authors showed that if grazing occurs at a corner, then the bifurcation is a BCB [50]. Subsequent studies revealed that so-called *grazing-sliding bifurcations* [58] and *event collisions* in systems with time-delayed switching [165] are also instances of BCBs. BCBs have been demonstrated experimentally in circuit systems [18, 207], and mechanical systems [150].

BCBs have been the subject of intense study over the past quarter century. A comprehensive description of BCBs in one dimension was given in [132, 149], and a classification of dynamics in the two-dimensional dissipative case was given in [17]. A wide variety of intricate dynamics may be created in BCBs. Recently several new features of BCBs have been identified, such as multi-dimensional attractors [95], and the simultaneous creation of infinitely many attractors [171]. Many investigations have been restricted to maps of one or two dimensions. This paper reviews BCBs emphasising properties and statements that hold in any number of dimensions.

In this paper we work with three different maps that each describe dynamics near a BCB, and are each useful in different contexts. In §3.1, to (1.2) we apply a coordinate change and expand f^L and f^R to produce the form

$$x_{i+1} = f(x_i;\mu,\eta) = \begin{cases} A_L(\eta)x_i + b(\eta)\mu + o\left(\|x_i\|,\mu\right) \ , & s_i \le 0 \\ A_R(\eta)x_i + b(\eta)\mu + o\left(\|x_i\|,\mu\right) \ , & s_i \ge 0 \end{cases} , \tag{1.3}$$

where $s = e_1^{\mathsf{T}} x$ denotes the first coordinate of $x \in \mathbb{R}^N$, $\mu \in \mathbb{R}$ is the primary bifurcation parameter, and $\eta \in \mathbb{R}^M$ represents other parameters of the map. Then by dropping the explicit nonlinear

terms in (1.3) we obtain the PWL approximation

$$x_{i+1} = g(x_i; \mu, \eta) = \begin{cases} A_L(\eta)x_i + b(\eta)\mu \ , & s_i \leq 0 \\ A_R(\eta)x_i + b(\eta)\mu \ , & s_i \geq 0 \end{cases} . \tag{1.4}$$

The validity of (1.4) is discussed in §3.2. Finally, under certain conditions detailed in §5, we can apply a second coordinate change such that A_L and A_R transform to companion matrices, and b transforms to e_1. The resulting PWL map (5.1) is referred to as the *border-collision normal form* (or observer canonical form). Roughly speaking, the three maps (1.3), (1.4) and (5.1) are increasingly easier to work with, but have increasingly more assumptions placed upon them.

The remainder of this paper is organised as follows. Applications and typical BCBs are discussed in §2. In §3 we introduce the maps (1.3) and (1.4) more carefully. In the subsequent four sections we study the map (1.4). Fixed points are analysed in §4, and the border-collision normal form is constructed in §5. Section 6 concerns periodic solutions. Any point of a periodic solution of (1.4) can be expressed as the solution to an $N \times N$ matrix equation. For this reason, we only need to employ elementary linear algebra to analyse non-degenerate periodic solutions created in BCBs. In particular, by considering only fixed points and period-two solutions, all generic BCBs can be categorised into exactly four distinct scenarios, as determined by the eigenvalues of A_L and A_R. More complicated attractors are discussed in §7.

In §8 we study the influence of the nonlinear terms dropped to produce (1.4) on non-hyperbolic fixed points and periodic solutions. Section 9 concerns the unique chain structure commonly exhibited by mode-locking regions of (1.3). Other dynamics such as invariant circles and homoclinic orbits are discussed in §10. Section 11 looks at special cases such as the one-dimensional case and the effects of smoothing and noise. Finally, §12 provides a summary and lookout for future studies.

2 The origin of continuous piecewise-linear maps

Return maps of nonsmooth systems of ODEs often take the general form (1.1). In this context, fixed points of (1.1) correspond to periodic orbits of the underlying ODE system. As parameters are varied a periodic orbit of the ODE system may develop an intersection with a switching manifold. This is a grazing event that corresponds to border-collision for (1.1). Several different types of grazing events have been classified [37, 52], and only in certain cases is the induced map locally continuous and asymptotically PWL, as required for a BCB. In this section we describe two such cases, indicate how BCBs can also occur for nonsmooth systems with time-delay in the switching condition, and illustrate typical BCBs.

2.1 Grazing-sliding bifurcations

Here we consider a PWS ODE system of the form:

$$\dot{X} = \begin{cases} F^L(X) \ , & H(X) < 0 \\ F^R(X) \ , & H(X) > 0 \end{cases} . \tag{2.1}$$

Subsets of the switching manifold $H(X) = 0$ that attract orbits from both sides are called *stable sliding regions*. Forward orbits of (2.1) that reach a stable sliding region subsequently evolve

on the region for some time. Such evolution is called *sliding motion* [73, 74, 188], and grazing events that involve sliding motion are called *sliding bifurcations*. Sliding bifurcations have been identified in models of mechanical systems with stick-slip friction [59, 98, 114], and various other applications [41, 44, 57, 185].

Several different types of sliding bifurcations have been classified [37, 58, 59, 107, 116]. At a *grazing-sliding bifurcation*, a periodic orbit of (2.1) has a quadratic tangency with the switching manifold at a point X^*, as shown in Fig. 1a. Given a suitable Poincaré section Π, the local induced return map $\mathcal{P} : \Pi \to \Pi$ is continuous and takes the form (1.2), where $x \in \Pi$. $\mathcal{P}$ is usually derived by composing global maps (describing motion from Π to a suitable cross-section intersecting X^*, and back), with a local *discontinuity map* that captures dynamics near X^* [52, 58].

In this scenario, one half-map of (1.2), say f^R, corresponds to orbits of (2.1) that connect x to $\mathcal{P}(x)$ along a path intersecting $H = 0$ near X^*, and the other half-map, f^L, corresponds to orbits for which there is no such intersection. Due to the quadratic tangency between the periodic orbit and $H = 0$, f^R admits an expansion in powers of $h(x)^{\frac{1}{2}}$. However, unlike for *regular grazing bifurcations* [51, 52], f^R has no square-root term (due to a cancellation of terms relating to the nature of sliding motion near X^*). Therefore (2.1) is PWL to leading order, and thus grazing-sliding bifurcations are examples of BCBs. In this instance f^R is differentiable but not C^2, so the unfolding theorems for codimension-two BCBs presented in §8 cannot usually be applied to grazing-sliding bifurcations.

Orbits of the ODE system corresponding to f^R involve segments of sliding motion near X^*. For this reason, the range of f^R is at most $(N-1)$-dimensional (where N is the dimension of Π). Consequently, the Jacobian $D_x f^R$ (denoted A_R in later sections) has a zero eigenvalue at the BCB. Furthermore, the local dynamics can be partially captured by an $(N-1)$-dimensional return map [92, 93].

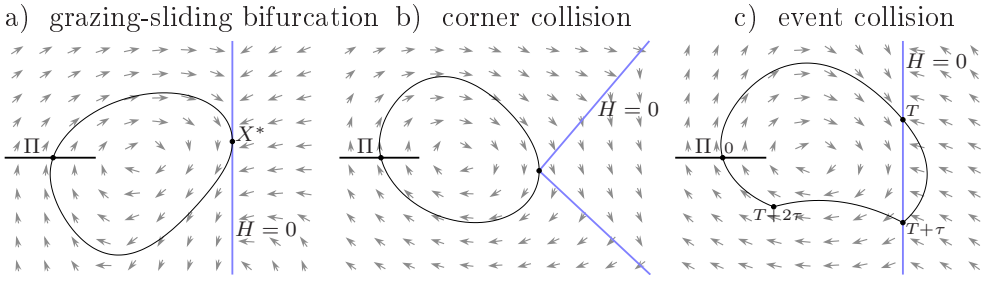

Figure 1: Three discontinuity-induced bifurcations of a periodic orbit of a PWS system of ODEs. Each of these are examples of BCBs. Each panel shows a schematic phase portrait illustrating the periodic orbit at the bifurcation. In each panel Π is a Poincaré section and $H = 0$ is a switching manifold. In panel (c) the switching condition has a time-delay τ, and evolution times at key points on the periodic orbit are indicated.

2.2 Corner collisions

For many reasons, switching manifolds of PWS systems of ODEs intersect or have a corner. Consider, for instance, the simple integrate-and-fire model

$$\dot{V} = -V + I - A\,\mathrm{sgn}\left(\sin\left(\frac{2\pi t}{T}\right)\right) , \qquad V(t^-) = 1 \;\Rightarrow\; V(t) = 0 , \tag{2.2}$$

where $V(t)$ represents the membrane potential of a neuron, I is a constant forcing current, and A and T denote the amplitude and period of square wave forcing [186]. When the value of V reaches 1, the neuron is said to fire and the value of V is reset to 0. Assuming $I > A > 0$, we can treat (2.2) as a two-dimensional PWS vector field with domain $(V, t) \in [0, 1) \times [0, T)$. In this setting the system has three switching manifolds, $V = 0$, $t = 0$ and $t = \frac{T}{2}$, that have two points of intersection.

DC/DC power converters employ high frequency switching for which current is permitted to flow for some variable fraction of the switching period. Simple mathematical models therefore typically often involve two switching manifolds: one for periodic switching events and one for times at which the current is halted, and these may intersect [49, 201]. In models of mechanical systems with compliant impacts, the switching manifold corresponds to points where objects impact or detach [123, 124, 129, 130, 150]. Detachment occurs when the contact force between objects vanishes. This provides a different algebraic expression for the switching manifold than points of impact, in which case the switching manifold often has a corner.

The collision of a periodic orbit with the corner of a switching manifold, or at the intersection of two manifolds, is referred to as a *corner collision*. Since corners and intersections constitute a measure zero subset of switching manifolds, one may suspect that corner collisions require an additional codimension to occur, but this is not the case. Simply visualise distortions of the periodic orbit shown in Fig. 1b. The periodic orbit generically attains an intersection with the switching manifold at the corner because the corner is a protuberance.

At a generic corner collision there is no tangency in the sense that no smooth component of the switching manifold is tangent to the periodic orbit at the bifurcation. For this reason, the induced return map $\mathcal{P} : \Pi \to \Pi$ is continuous and PWL to leading order [35, 50], and therefore corner collisions are also BCBs.

2.3 Event collisions in systems with time-delayed switching

We now consider (2.1) with constant time-delay in the switching condition:

$$\dot{X}(t) = \begin{cases} F^L(X(t)) , & H(X(t-\tau)) < 0 \\ F^R(X(t)) , & H(X(t-\tau)) > 0 \end{cases} . \tag{2.3}$$

In (2.3), $\tau > 0$ denotes the time-delay. Systems of the form (2.3) are used extensively to model switched control systems, both biological and man-made, where τ represents the inherent time lag between when variables are measured and the control is applied [29, 56, 153, 161].

Suppose an orbit of (2.3) crosses the switching manifold $H = 0$ at some time T. Then the functional form of the equations that govern evolution switches at the later time $t = T + \tau$. For a periodic orbit, the codimension-one phenomenon $H(X(T+\tau)) = 0$ is known as an *event collision*

[38], Fig. 1c. Generically the local induced return map $\mathcal{P} : \Pi \to \Pi$ is continuous and PWL to leading order [165]. Thus event collisions are BCBs, although due the presence of time-delay some care is required when defining Π. In some instances it is not possible to choose Π such that in a neighbourhood of the periodic orbit evolution through Π is independent to the location of the orbit at earlier times. In this case it may suffice to include the time since the last intersection with the switching manifold in the domain of the return map [166].

2.4 Typical border-collision bifurcations

To illustrate BCBs, we consider the system

$$\dot{X}(t) = \begin{cases} \mathcal{A}_L X(t) + \mathcal{B}_L \,, & U(t-\tau) < 0 \\ \mathcal{A}_R X(t) + \mathcal{B}_R \,, & U(t-\tau) > 0 \end{cases} , \tag{2.4}$$

where $X = (U, V, W)$, $\mathcal{A}_L$ and $\mathcal{A}_R$ are 3×3 matrices, and $\mathcal{B}_L, \mathcal{B}_R \in \mathbb{R}^3$. For simplicity we let Π coincide with $U = 0$, and only consider points on Π corresponding to orbits that previously resided in the left half-space ($U < 0$) for a continuous length of time equal to at least τ, see Fig. 2. The switching manifold of the induced return map $\mathcal{P} : \Pi \to \Pi$, is a curve on Π that separates points whose forward orbit reintersects $U = 0$ in a time less than τ, with points for which this time is greater than τ.

Fig. 3 shows numerically computed bifurcation diagrams of (2.4) using τ as the primary bifurcation parameter, and

$$\mathcal{A}_L = \begin{bmatrix} \eta & 1 & 0 \\ -2.5 & 0 & 1 \\ -3 & 0 & 0 \end{bmatrix} , \qquad \mathcal{B}_L = \begin{bmatrix} 0 \\ 0 \\ 1 \end{bmatrix} , \qquad \mathcal{A}_R = \mathbf{0} \,, \qquad \mathcal{B}_R = \begin{bmatrix} -1 \\ 1 \\ -1 \end{bmatrix} , \tag{2.5}$$

where $\eta \in \mathbb{R}$ is an additional parameter.

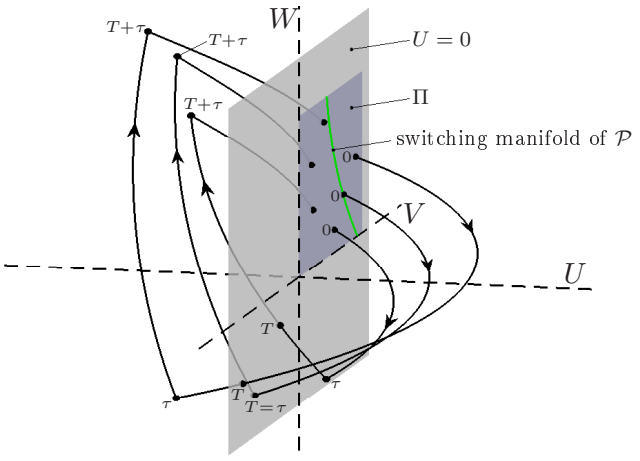

Figure 2: A sketch of the phase space of (2.4) showing three orbits beginning and ending on the Poincaré section Π. Evolution times at key points on the orbits are indicated. The orbits begin on Π at $t = 0$ and reintersect $U = 0$ at $t = T$.

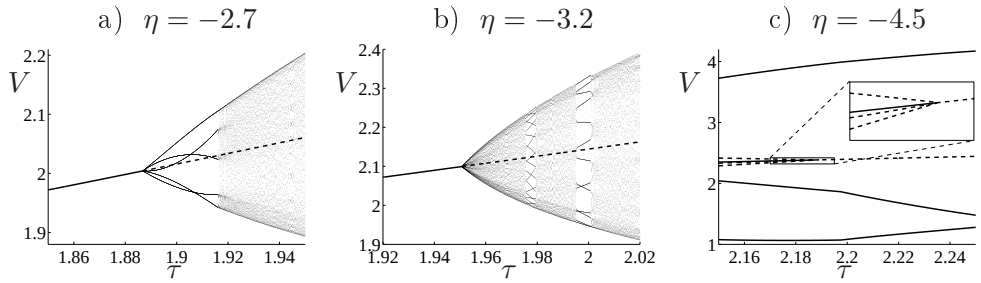

Figure 3: Three different BCBs (more specifically these are event collisions) for the system with time-delayed switching (2.4)-(2.5). The three panels show bifurcation diagrams corresponding to points on the Poincaré section Π ($U = 0$, see Fig. 2) for three different values of η. In each case an attracting periodic orbit (indicated by a solid curve) loses stability in a BCB (after which it is indicated by a dashed curve). The additional points in panels (a) and (b) were computed by numerically solving (2.4)-(2.5) and removing transient dynamics. In panel (c), an unstable 3-cycle exists to the left of the BCB (highlighted in the inset), and an attracting 3-cycle exists for all values of τ shown.

Over a range of values of η, (2.4)-(2.5) has an attracting periodic orbit that loses stability in a BCB:

i) With $\eta = -2.7$, the BCB occurs at $\tau \approx 1.8868$, Fig. 3a. At the bifurcation an attracting 5-cycle (a periodic orbit involving five loops near the original periodic orbit) is created. The 5-cycle is subsequently destroyed in a second BCB at $\tau \approx 1.9162$.

ii) With $\eta = -3.2$, numerics indicate that an attracting invariant circle is created at the BCB at $\tau \approx 1.9506$, Fig. 3b. Initially the dynamics on the invariant circle appears to be quasiperiodic. Mode-locking windows are visible for larger values of τ.

iii) With $\eta = -4.5$, numerics suggest that no attracting solution is created at the BCB at $\tau \approx 2.1878$, Fig. 3c. Prior to the bifurcation there exists a saddle-type 3-cycle, and the stable manifold of the 3-cycle appears to form the boundary of the basin of attraction of the attracting periodic orbit. As we approach the BCB, the periodic solution and 3-cycle coalesce and the size of the basin of attraction shrinks to zero. Beyond the BCB nearby orbits are attracted to another 3-cycle.

In each case, invariant sets created at the BCB grow in size asymptotically linearly with respect to τ. In §5.5 we return to this example after some essential properties of BCBs have been established.

3 Basic properties

In this section we begin by introducing local coordinates convenient for BCBs. This requires intuitive genericity assumptions that are justified by the implicit function theorem; further details are given in [17, 52]. We then introduce the PWL approximation and discuss adjugate matrices and invertibility.

3.1 Coordinate change and formulation

Suppose (1.1) has a BCB at $\mu = 0$, where $\mu \in \mathbb{R}$ is a parameter of (1.1), and $\eta \in \mathbb{R}^M$ represents all other parameters of (1.1). Also suppose that the switching manifold is smooth near the BCB. Then we can assume that the BCB occurs at the origin, and that locally the switching manifold coincides with the coordinate plane $s = 0$, where

$$s = e_1^{\mathsf{T}} x \ , \tag{3.6}$$

and e_j denotes the j^{th} standard basis vector of $\mathbb{R}^N$. Locally (1.1) may then be written as

$$x_{i+1} = f(x_i; \mu, \eta) = \begin{cases} f^L(x_i; \mu, \eta) \ , & s_i \leq 0 \\ f^R(x_i; \mu, \eta) \ , & s_i \geq 0 \end{cases} \ . \tag{3.7}$$

Since (3.7) is continuous and f^L and f^R are locally differentiable by assumption, we can write

$$f^J(x; \mu, \eta) = A_J(\eta)x + b(\eta)\mu + o\left(\|x\|, \mu\right) \ , \tag{3.8}$$

for $J = L, R$, where $b \in \mathbb{R}^N$, and A_L and A_R are $N \times N$ matrices. The requirement that (3.7) is continuous on $s = 0$, implies $e_j^{\mathsf{T}} A_L = e_j^{\mathsf{T}} A_R$ for all $j \neq 1$. That is,

$$A_R = A_L + \xi e_1^{\mathsf{T}} \ , \tag{3.9}$$

for some $\xi \in \mathbb{R}^N$.

3.2 The piecewise-linear approximation

With small values of x and μ, the linear terms dominate f^J. For this reason it is useful drop the higher order terms, with which (3.7)-(3.8) may be written as

$$x_{i+1} = g(x_i; \mu, \eta) = \begin{cases} g^L(x_i; \mu, \eta) \ , & s_i \leq 0 \\ g^R(x_i; \mu, \eta) \ , & s_i \geq 0 \end{cases} \ , \tag{3.10}$$

where

$$g^J(x; \mu, \eta) = A_J(\eta)x + b(\eta)\mu \ . \tag{3.11}$$

The maps (3.7)-(3.8) and (3.10)-(3.11) were stated as (1.3) and (1.4) in §1, and for the remainder of the paper we refer to (1.3) and (1.4).

For any $\lambda > 0$, we have $g(\lambda x; \lambda\mu, \eta) = \lambda g(x; \mu, \eta)$. Consequently, all bounded invariant sets of (1.4) collapse linearly to the origin as $\mu \to 0$. For the purposes of determining the dynamics of (1.4), it suffices to consider $\mu \in \{-1, 0, 1\}$. Furthermore, if we are willing to switch L and R, we can further ignore the case $\mu = -1$ because (1.4) is unchanged under the replacement

$$(x, \mu, L, R) \mapsto (-x, -\mu, R, L) \ . \tag{3.12}$$

To justify (1.4) for use as an approximation to (1.3), suppose Ω is a bounded invariant set of $g(x; 1, \eta)$. Then for all $\mu > 0$, $\mu\Omega$ is a bounded invariant set of $g(x; \mu, \eta)$. By choosing a suitably small value $\mu > 0$, we can make the difference between the right-hand sides of (1.3) and (1.4) as small as we like in a neighbourhood of $\mu\Omega$. If Ω is a *structurally stable* invariant set of $g(x; 1, \eta)$, then for sufficiently small $\mu > 0$ some perturbation of $\mu\Omega$ is an invariant set of (1.3).

3.3 Adjugate matrices

Many basic calculations for (1.4) involve *adjugate matrices* [23, 112]. Given an $N \times N$ matrix A, let m_{ij} denote the determinant of the $(N-1) \times (N-1)$ matrix formed by removing the i^{th} row and j^{th} column from A (the m_{ij} are called the *minors* of A). The adjugate of A is then defined by $\text{adj}(A)_{ij} = (-1)^{i+j} m_{ji}$. It is a standard linear algebra exercise to show that for any A

$$\text{adj}(A)A = A\,\text{adj}(A) = \det(A) I \ . \tag{3.13}$$

If A is nonsingular then $A^{-1} = \frac{\text{adj}(A)}{\det(A)}$.

Given any $\xi \in \mathbb{R}^N$, $A + \xi e_1^{\mathsf{T}}$ differs from A in only the first column. By changing only the first column of A, each m_{i1} is unchanged and hence the first row of the adjugate is unchanged, i.e.,

$$e_1^{\mathsf{T}} \text{adj}\left(A + \xi e_1^{\mathsf{T}}\right) = e_1^{\mathsf{T}} \text{adj}(A) \ . \tag{3.14}$$

3.4 Invertibility

In order to construct the inverse of (1.4), we let

$$\varphi^{\mathsf{T}} = e_1^{\mathsf{T}} \text{adj}(A_L) = e_1^{\mathsf{T}} \text{adj}(A_R) \ . \tag{3.15}$$

The second equality in (3.15) is a consequence of (3.9) and (3.14). By using (3.13), we obtain

$$\varphi^{\mathsf{T}} g(x) = \begin{cases} \det(A_L) s + \varphi^{\mathsf{T}} b\mu \ , & s \le 0 \\ \det(A_R) s + \varphi^{\mathsf{T}} b\mu \ , & s \ge 0 \end{cases} \ . \tag{3.16}$$

Therefore if $s \le 0$ and $\det(A_L) \neq 0$, then $s = \frac{\varphi^{\mathsf{T}}(g(x) - b\mu)}{\det(A_L)}$, and if $s \ge 0$ and $\det(A_R) \neq 0$, then $s = \frac{\varphi^{\mathsf{T}}(g(x) - b\mu)}{\det(A_R)}$. It follows that (1.4) is invertible if and only if $\det(A_L A_R) > 0$, in which case

$$g^{-1}(x) = \begin{cases} A_L^{-1}(x - b\mu) \ , & \frac{\varphi^{\mathsf{T}}(x - b\mu)}{\det(A_L)} \le 0 \\ A_R^{-1}(x - b\mu) \ , & \frac{\varphi^{\mathsf{T}}(x - b\mu)}{\det(A_R)} \ge 0 \end{cases} \ . \tag{3.17}$$

4 Fixed points

Here we work with the PWL map (1.4). If the matrices $I - A_L$ and $I - A_R$ are nonsingular, then (1.4) has two possible fixed points:

$$x^J = (I - A_J)^{-1} b\mu \ , \tag{4.1}$$

for $J = L, R$. Each x^J is a fixed point of (1.4), and said to be *admissible*, if it lies on the appropriate side of $s = 0$, or on $s = 0$, otherwise it is said to be *virtual*. That is, x^L is admissible if and only if $s^L \le 0$, and x^R is admissible if and only if $s^R \ge 0$.

We let

$$\varrho^{\mathsf{T}} = e_1^{\mathsf{T}} \text{adj}(I - A_L) = e_1^{\mathsf{T}} \text{adj}(I - A_R) \ , \tag{4.2}$$

where we have used (3.14) to obtain the second equality. By multiplying both sides of (4.1) by e_1^T on the left, we obtain

$$s^J = \frac{\varrho^\mathsf{T} b}{\det(I - A_J)}\mu \, . \tag{4.3}$$

Therefore if $I - A_L$ and $I - A_R$ are nonsingular, then as μ is varied from zero the two fixed points move away from $s = 0$ if and only if $\varrho^\mathsf{T} b \neq 0$. Hence

$$\varrho^\mathsf{T} b \neq 0 \, , \tag{4.4}$$

is a non-degeneracy condition for the BCB at $\mu = 0$.

4.1 Persistence versus nonsmooth folds

The admissibility of x^L and x^R is determined by the signs of s^L and s^R. From (4.3) we see that there are two distinct scenarios (assuming $I - A_L$ and $I - A_R$ are nonsingular and $\varrho^\mathsf{T} b \neq 0$).

i) If $\det(I - A_L)$ and $\det(I - A_R)$ have the same sign, then x^L and x^R are admissible for different signs of μ, and thus (1.4) has a unique fixed point for all $\mu \in \mathbb{R}$. This case is referred to as *persistence*, Fig. 4a.

ii) If $\det(I - A_L)$ and $\det(I - A_R)$ have different signs, then x^L and x^R are admissible for the same sign of μ. The two fixed points of (1.4) collide and annihilate at the origin at $\mu = 0$ in a manner akin to a saddle-node bifurcation. This case is referred to as a *nonsmooth fold*, Fig. 4b.

4.2 Feigin's classification, part I

Here we demonstrate how BCBs can be classified as either persistence or a nonsmooth fold by looking at the eigenvalues of A_L and A_R. This was first described by Feigin in [70]. (The analogous classification of period-2 solutions is given in §6.6, following a general discussion of periodic solutions.)

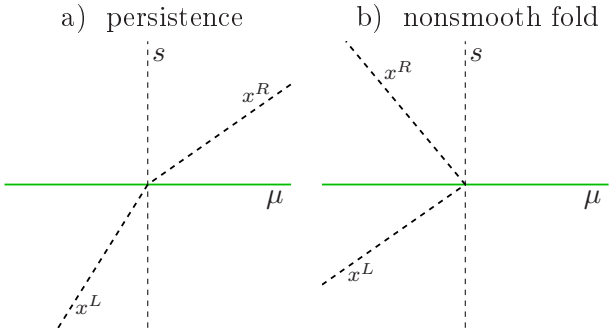

Figure 4: Two bifurcation diagrams of (1.4) showing the fixed points x^L and x^R (4.1). All generic BCBs conform to one of these two scenarios.

Let σ_J^+ denote the number of real eigenvalues of A_J that are greater than 1. If $I - A_J$ is nonsingular (equivalently, if 1 is not an eigenvalue of A_J), then

$$\operatorname{sgn}\left(\det(I - A_J)\right) = (-1)^{\sigma_J^+} \ . \tag{4.5}$$

Then by (4.3) we have

$$\operatorname{sgn}\left(s^J\right) = (-1)^{\sigma_J^+} \operatorname{sgn}\left(\varrho^{\mathsf{T}} b\mu\right) \ , \tag{4.6}$$

from which the next result immediately follows.

Proposition 4.1. *Suppose $\varrho^{\mathsf{T}} b \neq 0$ and 1 is not an eigenvalue of A_L or A_R. If $\sigma_L^+ + \sigma_R^+$ is even [odd], then $\mu = 0$ corresponds to persistence [a nonsmooth fold].*

5 The border-collision normal form

As with classical bifurcations of smooth dynamical systems, it is often convenient to work with a normal form. A normal or canonical form for (1.4) is:

$$x_{i+1} = \begin{cases} C_L x_i + e_1 \mu \ , & s_i \leq 0 \\ C_R x_i + e_1 \mu \ , & s_i \geq 0 \end{cases} \ , \tag{5.1}$$

where C_L and C_R are companion matrices

$$C_J = \left[-\Delta_J \,\middle|\, \frac{I}{0 \cdots 0} \right] \ , \tag{5.2}$$

where $\Delta_J \in \mathbb{R}^N$, and I is the $(N-1) \times (N-1)$ identity matrix. The map (5.1) is known as the *border-collision normal form*, although slight variations of (5.1)-(5.2) have been used by different authors. In the special case $N = 2$, it is convenient to write

$$C_J = \begin{bmatrix} \tau_J & 1 \\ -\delta_J & 0 \end{bmatrix} \ , \tag{5.3}$$

because τ_J and δ_J are, respectively, the trace and determinant of C_J.

For a given PWL map (1.4), we would like to transform it to (5.1) via an invertible affine coordinate change

$$x \mapsto Tx + q\mu \ , \qquad \mu \mapsto a\mu \ , \tag{5.4}$$

that does not disrupt the first coordinate of x. This requires $e_1^{\mathsf{T}} T = e_1^{\mathsf{T}}$, $e_1^{\mathsf{T}} q = 0$, $\det(T) \neq 0$ and $a \neq 0$. Below we explain that such a coordinate change is possible if and only if (1.4) is *observable* and $\varrho^{\mathsf{T}} b \neq 0$. This was essentially first achieved in $\mathbb{R}^N$ by di Bernardo [48]. The terminology stems from the derivation of the continuous-time analogue of (5.1) through the use of control theory concepts [31, 60].

The border-collision normal form (5.1) is convenient to work with for several reasons. In addition to μ, there are exactly $2N$ parameters (these are the elements of the vectors Δ_L and Δ_R). The coefficients of the characteristic polynomial of C_J are given by the elements of Δ_J:

$$\det(\lambda I - C_J) = \lambda^N + \Delta_{J,1}\lambda^{N-1} + \cdots + \Delta_{J,N-1}\lambda + \Delta_{J,N} \ . \tag{5.5}$$

The map (5.1) automatically satisfies the non-degeneracy condition (4.4), because $\varrho^{\mathsf{T}} = [1, \ldots, 1]$ and $b = e_1$.

5.1 Observability

Consider for a moment the linear map $x_{i+1} = A_L x_i$. Given some x_0, we can iterate this map to determine all future points x_i. But suppose that we are instead given some values $s_i = e_1^\mathsf{T} x_i$ (these represent our observations of the system). If we can always determine x_0 from $s_0, \ldots, s_{N-1}$, then the pair $\left(A_L, e_1^\mathsf{T}\right)$ is said to be *observable* [67, 178, 187, 192]. The values $s_0, \ldots, s_{N-1}$ are the elements of the vector $\mathcal{O}_L x_0$, where

$$\mathcal{O}_J = \begin{bmatrix} e_1^\mathsf{T} A_J^{N-1} \\ \vdots \\ e_1^\mathsf{T} A_J \\ e_1^\mathsf{T} \end{bmatrix} , \tag{5.6}$$

for $J = L, R$. Therefore $\left(A_L, e_1^\mathsf{T}\right)$ is observable if and only if $\mathcal{O}_L$ is nonsingular.

The following result relates $\mathcal{O}_L$ to the desired coordinate change (5.4) and can be proved with only basic linear algebra tools, but this does require some ingenuity, see [22, 168].

Lemma 5.1. *There exists a nonsingular matrix T, with $e_1^\mathsf{T} T = e_1^\mathsf{T}$, such that $T A_L T^{-1}$ is a companion matrix of the form (5.2), if and only if $\mathcal{O}_L$ is nonsingular.*

In view of Lemma 5.1, we say that (1.4) is *observable* if $\mathcal{O}_L$ is nonsingular. In view of the next result, which is a consequence of the identity (3.9) and can be deduced from Lemma 5.1 in a few lines, observability of (1.4) could equally be defined using $\mathcal{O}_R$.

Lemma 5.2. *$\mathcal{O}_L$ is nonsingular if and only if $\mathcal{O}_R$ is nonsingular.*

5.2 Construction of the affine transformation

The following result provides us with an explicit expression for the transformation (5.4).

Proposition 5.3. *Suppose $\mathcal{O}_L$ is nonsingular. Let*

$$\begin{aligned} T &= \left[A_L^{N-1} \mathcal{O}_L^{-1} e_1 \middle| \cdots \middle| A_L \mathcal{O}_L^{-1} e_1 \middle| \mathcal{O}_L^{-1} e_1 \right]^{-1} , \\ q &= (I - C)^{-1} \left(e_1 \varrho^\mathsf{T} - T \right) b , \\ a &= \varrho^\mathsf{T} b , \end{aligned} \tag{5.7}$$

for any companion matrix C of the form (5.2) for which $I - C$ is nonsingular. Then under the transformation (5.4), (1.4) transforms to (5.1).

We leave a proof of Proposition 5.3, and a verification that $e_1^\mathsf{T} T = e_1^\mathsf{T}$ and $e_1^\mathsf{T} q = 0$ to the reader. This may be achieved via direct calculations. For the matrix C that appears in (5.7), we could use C_L or C_R if possible, or we could simply use the companion matrix for which $\Delta = 0$. If $\varrho^\mathsf{T} b = 0$ for (1.4), then the behaviour of (5.1) for $\mu \neq 0$ does not match the behaviour of (1.4) for $\mu \neq 0$.

5.3 The unobservable case

If (1.4) is not observable then it may be decoupled [67]. Specifically, after an affine coordinate change, we can write $x = (\tilde{x}, \tilde{y})$, where $\tilde{x} \in \mathbb{R}^{N-j}$ and $\tilde{y} \in \mathbb{R}^j$, such that (1.4) takes the form

$$\begin{aligned} \tilde{x}_{i+1} &= \tilde{g}(\tilde{x}_i) \ , \\ \tilde{y}_{i+1} &= \psi_1(\tilde{y}_i) + \psi_2(\tilde{x}_i) \ , \end{aligned} \tag{5.8}$$

where $\tilde{g}$ and ψ_2 are PWL, and ψ_1 is affine. Evolution of $\tilde{x}$ is governed by the $(N-j)$-dimensional PWL map $\tilde{g}$. Therefore in this case we can obtain a partial description of the dynamics by working in a lower number of dimensions.

5.4 Consequences of the border-collision normal form

A geometric interpretation of observability is provided by the *Popov-Belevitch-Hautus observability test* [155, 178, 195]. In our context, this control theory result states that (1.4) is observable if and only if A_L does not have an eigenvector orthogonal to e_1. The test can be used to quickly ascertain observability in some scenarios. For instance, if A_L has a repeated real-valued eigenvalue with a corresponding eigenspace that is at least two-dimensional, then A_L must have an eigenvector orthogonal to e_1, and so (1.4) cannot be observable. Alternatively, if (1.4) is two-dimensional and A_L has complex eigenvalues, then (1.4) must be observable.

Next, let us make two elementary, but important, observations:

i) The dynamics of (5.1) for all $\mu \in \mathbb{R}$ is determined by the coefficients of the characteristic polynomials of C_L and C_R.

ii) These coefficients are determined by the eigenvalues of C_L and C_R (taking the algebraic multiplicity of the eigenvalues into account).

Furthermore, by Proposition 5.3, if $\mathcal{O}_L$ is nonsingular and $\varrho^{\mathsf{T}} b \neq 0$, then under the transformation (5.4):

iii) The dynamics of (5.1) is affinely conjugate to the dynamics of (1.4).

iv) C_L and C_R are similar to A_L and A_R, respectively.

These four facts lead us to the following fundamental conclusion: if (1.4) is observable and $\varrho^{\mathsf{T}} b \neq 0$, then *the dynamics of (1.4) for all $\mu \in \mathbb{R}$ is determined by the eigenvalues of A_L and A_R*.

Next we use this result to help us understand BCBs of the system introduced in §2.4. Note also that the eigenvalues of A_L and A_R are the stability multipliers of the fixed points x^L and x^R, if they exist.

5.5 An example

Here we use the above results to explain some aspects of Fig. 3. Local to a BCB the return map $\mathcal{P} : \Pi \to \Pi$ of (2.4)-(2.5) is asymptotically PWL, but, as discussed above, in order to determine the dynamics created in the bifurcation we expect that we only need to compute the eigenvalues

of the left and right linearisations. We do not have to put $\mathcal{P}$ in the form (1.3) and compute all the elements of A_L, A_R and b, unless we want to quantitatively match the dynamics of the border-collision normal form (5.1) with the dynamics of (2.4)-(2.5), or unless we want to formally verify observability and the non-degeneracy condition $\varrho^{\mathsf{T}} b \neq 0$.

The eigenvalues of the left and right linearisations of $\mathcal{P}$ can be estimated by computing finite difference approximations to numerical solutions of (2.4)-(2.5). For the three BCBs of Fig. 3, to four decimal places, the eigenvalues of C_L and C_R are

a) $\lambda^L_{1,2} = -0.5920 \pm 0.4639\mathrm{i}, \quad \lambda^R_{1,2} = -0.8870 \pm 0.6206\mathrm{i},$

b) $\lambda^L_{1,2} = -0.5109 \pm 0.5385\mathrm{i}, \quad \lambda^R_{1,2} = -0.9526 \pm 0.7236\mathrm{i},$

c) $\lambda^L_{1,2} = -0.3897 \pm 0.6167\mathrm{i}, \quad \lambda^R_{1,2} = -1.2502, -2.2244,$

where we have chosen the right half-map to correspond to orbits of (2.4)-(2.5) that return to $U = 0$ in a time less than τ. In each case $|\lambda^L_{1,2}| < 1$, thus prior to the BCB the periodic orbit is attracting. Similarly, in each case $|\lambda^R_{1,2}| > 1$, thus after the BCB the periodic orbit is repelling. Furthermore, in each case $\sigma^+_L + \sigma^+_R = 0$, thus by Proposition 4.1 each BCB corresponds to persistence, as evident in Fig. 3.

With the first combination of eigenvalues (corresponding to $\eta = -2.7$ and Fig. 3a), $\mathcal{P}$ corresponds to (5.1) with

$$\Delta_L = [1.1840, 0.5657]^{\mathsf{T}}, \qquad \Delta_R = [1.7740, 1.1719]^{\mathsf{T}}, \tag{5.9}$$

to four decimal places. Fig. 5 shows a bifurcation diagram of (5.1) with (5.9). An attracting 5-cycle is created at $\mu = 0$. The 5-cycle is a structurally stable invariant set, thus is exhibited by $\mathcal{P}$ for a small interval of values of τ immediately beyond the BCB, and this can be seen in Fig. 3a. We may formally verify the existence of an attracting 5-cycle for (5.1) by studying fixed points of the fifth iterate of (5.1), as discussed in the next section.

6 Periodic solutions

PWL maps are extremely convenient to work with in regards to periodic solutions. Any point of a periodic solution of (1.4) is the fixed point of some composition of g^L and g^R. Since g^L and g^R

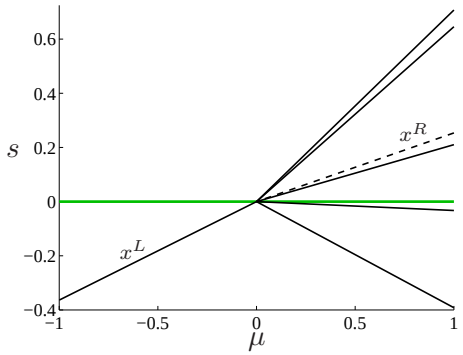

Figure 5: A bifurcation diagram of (5.1) with (5.9). Solid [dashed] lines indicate a stable [unstable] solution. For $\mu > 0$ the solid lines represent a stable 5-cycle.

are affine, any such composition is also affine. Thus the problem of finding a periodic solution reduces to solving a linear system of algebraic equations.

6.1 Symbolic representation

We associate an orbit of (1.4), $\{x_i\}$, with a symbol sequence, $\mathcal{S} : \mathbb{Z} \to \{L, R\}$, by setting $\mathcal{S}_i = L$ if $s_i < 0$, and $\mathcal{S}_i = R$ if $s_i > 0$. If $s_i = 0$ we impose no restriction on $\mathcal{S}_i$ because (1.4) is continuous (some authors introduce a third symbol in this case).

If $\{x_i\}$ is periodic with period n, then the corresponding symbol sequence $\mathcal{S}$ is the infinite repetition of the word $\mathcal{S}_0 \cdots \mathcal{S}_{n-1}$. For this reason, whenever we write a periodic symbol sequence, we just list the symbols $\mathcal{S}_0 \cdots \mathcal{S}_{n-1}$. We use the notation $\mathcal{S}^{(i)}$ to denote the i^{th} left shift permutation of $\mathcal{S}$ (i.e., $\mathcal{S}^{(i)}_j \equiv \mathcal{S}_{i+j}$), and let $\mathcal{S}^{\overline{i}}$ denote the symbol sequence created by changing the symbols $\mathcal{S}_{i+jn}$, for all $j \in \mathbb{Z}$. For example, for the periodic solution in Fig. 5, if we choose x_0 to denote the point of the periodic solution with the smallest value of s, then the corresponding symbol sequence is $\mathcal{S} = LRLRR$. Then, for instance, $\mathcal{S}^{(2)} = LRRLR$ and $\mathcal{S}^{\overline{2}} = LRRRR$.

6.2 Existence and uniqueness

Let $\mathcal{S}$ be a periodic symbol sequence, and let $n \in \mathbb{Z}^+$ be a period of $\mathcal{S}$. Write $n = kn_{\min}$, where $k \in \mathbb{Z}^+$ and $n_{\min}$ is the minimal period of $\mathcal{S}$. We refer to an n-tuple, $\left\{x_i^{\mathcal{S}}\right\}_{i=0}^{n-1}$, that satisfies

$$x^{\mathcal{S}}_{(i+1) \bmod n} = g^{\mathcal{S}_i}\left(x_i^{\mathcal{S}}\right) \ , \tag{6.1}$$

for all i, as an $\mathcal{S}^{[k]}$-cycle, or just an $\mathcal{S}$-cycle if it is clear what value of k is being used (usually $k = 1$). In order to compute $\mathcal{S}$-cycles of (1.4), we let $g^{\mathcal{S}} = g^{\mathcal{S}_{n-1}} \circ \cdots \circ g^{\mathcal{S}_0}$. The map $g^{\mathcal{S}}$ is affine and given by

$$g^{\mathcal{S}}(x) = M_{\mathcal{S}} x + P_{\mathcal{S}} b\mu \ , \tag{6.2}$$

where

$$M_{\mathcal{S}} = A_{\mathcal{S}_{n-1}} \cdots A_{\mathcal{S}_0} \ , \tag{6.3}$$

$$P_{\mathcal{S}} = I + A_{\mathcal{S}_{n-1}} + A_{\mathcal{S}_{n-1}} A_{\mathcal{S}_{n-2}} + \cdots + A_{\mathcal{S}_{n-1}} \cdots A_{\mathcal{S}_1} \ . \tag{6.4}$$

Each $x_i^{\mathcal{S}}$ is a fixed point of $g^{\mathcal{S}^{(i)}}$, that is

$$\left(I - M_{\mathcal{S}^{(i)}}\right) x_i^{\mathcal{S}} = P_{\mathcal{S}^{(i)}} b\mu \ . \tag{6.5}$$

Therefore if $I - M_{\mathcal{S}^{(i)}}$ is nonsingular, or equivalently if 1 is not an eigenvalue of $M_{\mathcal{S}^{(i)}}$, then $x_i^{\mathcal{S}}$ is unique. If $I - M_{\mathcal{S}^{(i)}}$ is singular, $x_i^{\mathcal{S}}$ either does not exist or is non-unique. It is a straight-forward exercise to show that the spectrum of $I - M_{\mathcal{S}^{(i)}}$ is independent of i, because changing i only changes the cyclical order in which A_L and A_R are multiplied to form $M_{\mathcal{S}^{(i)}}$. These observations provide us with the following result.

Proposition 6.1. *The $\mathcal{S}$-cycle is unique if and only if $I - M_{\mathcal{S}}$ is nonsingular, and if $I - M_{\mathcal{S}}$ is nonsingular then*

$$x_i^{\mathcal{S}} = \left(I - M_{\mathcal{S}^{(i)}}\right)^{-1} P_{\mathcal{S}^{(i)}} b\mu \ . \tag{6.6}$$

It usually suffices to consider $k = 1$ for the following reason. Suppose $M_{\mathcal{S}}$ with $n = n_{\min}$ does not have an eigenvalue with unit modulus, as is generically the case. Then by Proposition 6.1, the $\mathcal{S}^{[1]}$-cycle is unique. For any $k \in \mathbb{Z}^+$, the matrix part of $g^{\mathcal{S}_{kn_{\min}-1}} \circ \cdots \circ g^{\mathcal{S}_0}$ is equal to $M_{\mathcal{S}}^k$. Since 1 is not an eigenvalue of $M_{\mathcal{S}}^k$, the $\mathcal{S}^{[k]}$-cycle is also unique. The $\mathcal{S}^{[1]}$ and $\mathcal{S}^{[k]}$-cycles satisfy the same set of equations (6.1), therefore they consist of the same points. For this reason it is not helpful to further study the $\mathcal{S}^{[k]}$-cycle. If $M_{\mathcal{S}}$ does have an eigenvalue with unit modulus, then $\mathcal{S}$-cycles with $k > 1$ can be important, see §8.

6.3 Admissibility

An $\mathcal{S}$-cycle is a periodic solution of (1.4) only if each point of the $\mathcal{S}$-cycle lies on the "correct" side of the switching manifold, or on the switching manifold. That is, $s_i^{\mathcal{S}} \leq 0$ whenever $\mathcal{S}_i = L$ and $s_i^{\mathcal{S}} \geq 0$ whenever $\mathcal{S}_i = R$. In this case the $\mathcal{S}$-cycle is said to be *admissible*; otherwise it is *virtual*.

To study the admissibility of $\mathcal{S}$-cycles, it is useful to use the identity

$$e_1^{\mathsf{T}} \mathrm{adj}\,(I - M_{\mathcal{S}^{(i)}})\, P_{\mathcal{S}^{(i)}} = \det\,(P_{\mathcal{S}^{(i)}})\, \varrho^{\mathsf{T}}\ , \tag{6.7}$$

where ϱ is given by (4.2). Equation (6.7) is a non-trivial consequence of the requirement that A_L and A_R differ in only their first columns. For a derivation refer to [168, 175]. By multiplying both sides of (6.5) by $e_1^{\mathsf{T}}\mathrm{adj}(I - M_{\mathcal{S}^{(i)}})$ on the left, and applying (6.7), we obtain

$$\det(I - M_{\mathcal{S}}) s_i^{\mathcal{S}} = \det\,(P_{\mathcal{S}^{(i)}})\, \varrho^{\mathsf{T}} b\mu\ . \tag{6.8}$$

The next result follows immediately from (6.8).

Proposition 6.2. *i) If $\mu \neq 0$, $\varrho^{\mathsf{T}} b \neq 0$ and $I - M_{\mathcal{S}}$ is singular, yet $g^{\mathcal{S}}$ has a fixed point, then $P_{\mathcal{S}^{(i)}}$ is singular for all i.*

ii) If $I - M_{\mathcal{S}}$ is nonsingular, then

$$s_i^{\mathcal{S}} = \frac{\det\,(P_{\mathcal{S}^{(i)}})\, \varrho^{\mathsf{T}} b\mu}{\det(I - M_{\mathcal{S}})}\ . \tag{6.9}$$

From part (i) of Proposition 6.2 we can say that if $I - M_{\mathcal{S}}$ is singular and $P_{\mathcal{S}}$ is nonsingular, then $g^{\mathcal{S}}$ does not have a fixed point and so no $\mathcal{S}$-cycle exists. From part (ii) of Proposition 6.2 we can relate the admissibility of an $\mathcal{S}$-cycle to the determinants of the $P_{\mathcal{S}^{(i)}}$:

Proposition 6.3. *Suppose $I - M_{\mathcal{S}}$ is nonsingular, $\mu \neq 0$, and $\varrho^{\mathsf{T}} b \neq 0$. Let $\gamma = \mathrm{sgn}\left(\frac{\varrho^{\mathsf{T}} b\mu}{\det(I - M_{\mathcal{S}})}\right)$. Then the $\mathcal{S}$-cycle is an admissible periodic solution of (1.4) if and only if, for all values of i for which $P_{\mathcal{S}^{(i)}}$ is nonsingular:*

$$\begin{aligned} \text{if } \mathcal{S}_i = L,\ \text{then } \mathrm{sgn}\,(\det\,(P_{\mathcal{S}^{(i)}})) &= -\gamma\ , \\ \text{if } \mathcal{S}_i = R,\ \text{then } \mathrm{sgn}\,(\det\,(P_{\mathcal{S}^{(i)}})) &= \gamma\ . \end{aligned}$$

6.4 Stability

If no points of an $\mathcal{S}$-cycle lie on the switching manifold, then the image of a suitably small neighbourhood of $x_0^{\mathcal{S}}$ under n iterations of (1.4) is given by $g^{\mathcal{S}}$. Therefore the evolution of points near $x_0^{\mathcal{S}}$ is determined by $M_{\mathcal{S}}$, and the stability of the $\mathcal{S}$-cycle is determined by the eigenvalues of $M_{\mathcal{S}}$.

Proposition 6.4. *An admissible $\mathcal{S}$-cycle of (1.4) with no points on the switching manifold is attracting [stable] if and only if all eigenvalues of $M_{\mathcal{S}}$ have modulus less than 1 [less than or equal to 1].*

Furthermore, by (6.8) if an $\mathcal{S}$-cycle has no points on the switching manifold and $I - M_{\mathcal{S}}$ is nonsingular, then $\mu \neq 0$, $\varrho^{\mathsf{T}} b \neq 0$, and $P_{\mathcal{S}^{(i)}}$ is nonsingular for all i. If in addition $M_{\mathcal{S}}$ has no eigenvalues with modulus 1, then the $\mathcal{S}$-cycle is hyperbolic and structurally stable.

6.5 A four-dimensional example

As an example, we consider (5.1) with

$$\Delta_L = [-\tau_L,\, 0,\, 0,\, \delta_L]^{\mathsf{T}} \;, \quad \Delta_R = [-\tau_R,\, 4,\, 0,\, \delta_R]^{\mathsf{T}} \;, \tag{6.10}$$

and search for parameters $\tau_L, \delta_L, \tau_R, \delta_R \in \mathbb{R}$ yielding an attracting LLR-cycle for $\mu > 0$. With $\mathcal{S} = LLR$, by (6.3) and (6.4) we have $M_{\mathcal{S}} = A_R A_L^2$ and $P_{\mathcal{S}} = I + A_R + A_R A_L$, where A_L and A_R are the companion matrices (5.2). In Proposition 6.3 we use $\gamma = 1$ because

i) we are considering $\mu > 0$,

ii) we require $\det(I - M_{\mathcal{S}}) > 0$ for the LLR-cycle to be attracting, and

iii) $\varrho^{\mathsf{T}} b = 1$, since is the map is in border-collision normal form.

Therefore by Proposition 6.3 the $\mathcal{S}$-cycle is admissible if

$$\det(P_{\mathcal{S}}) < 0 \;, \quad \det\left(P_{\mathcal{S}^{(1)}}\right) < 0 \;, \quad \det\left(P_{\mathcal{S}^{(2)}}\right) > 0 \;. \tag{6.11}$$

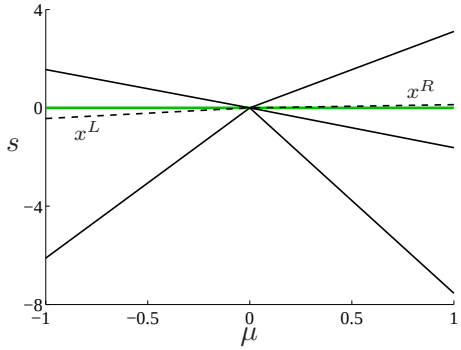

Figure 6: A bifurcation diagram of the border-collision normal form (5.1) with (6.10) and (6.12). For $\mu < 0$ the fixed point x^L is unstable and there exists a stable LR-cycle. For $\mu > 0$ the fixed point x^R is unstable and there exists a stable LLR-cycle.

Direct calculations with (6.10) yield

$$\begin{aligned}
\det(I - M_{\mathcal{S}}) &= 4\tau_L - 4\delta_L + \delta_L^2\delta_R + \delta_R\tau_L^2 - \delta_L^2\tau_R - \tau_L^2\tau_R - 2\delta_L\delta_R\tau_L + 2\delta_L\tau_L\tau_R + 1 \,, \\
\det(P_{\mathcal{S}}) &= 4\tau_L - \delta_R - 4\delta_L + \tau_R + \delta_L\delta_R - \delta_L\tau_R - \delta_R\tau_L + \tau_L\tau_R + 1 \,, \\
\det\left(P_{\mathcal{S}^{(1)}}\right) &= \tau_L - \delta_L + \delta_L\delta_R - \delta_L\tau_R - \delta_R\tau_L + \tau_L\tau_R - 3 \,, \\
\det\left(P_{\mathcal{S}^{(2)}}\right) &= \delta_L^2 - 2\delta_L\tau_L - \delta_L + \tau_L^2 + \tau_L + 1 \,.
\end{aligned}$$

Numerically we can use these expressions to find parameter values where (6.11) holds. For example, (6.11) holds with

$$\tau_L = -\frac{3}{2} \,, \quad \delta_L = -\frac{1}{5} \,, \quad \tau_R = -\frac{5}{2} \,, \quad \delta_R = \frac{1}{4} \,. \tag{6.12}$$

and at these parameter values the LLR-cycle is attracting, see Fig. 6. With (6.12) and $\mu < 0$, the map has an attracting LR-cycle. The reader may verify this for themselves using the above methodology, however, for period-two solutions there is a simpler approach as discussed in the next section.

This example highlights some general idiosyncrasies encountered when analysing dynamics near a BCB for a map with many parameters. Since we have explicit expressions for $M_{\mathcal{S}}$ and $P_{\mathcal{S}^{(i)}}$ in terms of A_L and A_R, which contain the parameters, it is relatively easy to numerically identify parameter regions where $\mathcal{S}$-cycles are admissible. However, explicit expressions for $\det\left(P_{\mathcal{S}^{(i)}}\right)$ are relatively complicated, except in simple cases such as $N = 1$, so it is impractical to describe these regions analytically. Indeed it is futile to attempt a complete classification of the dynamics of (5.1) in terms of the $2N$ parameters $\Delta_{J,i}$. Nevertheless a partial classification can be useful. For instance in the two-dimensional dissipative case ($N = 2$ and $|\det(A_L)|, |\det(A_R)| < 1$), eleven fundamentally different scenarios have been identified explicitly in terms of the parameters of (5.1) [17, 19].

6.6 Feigin's classification, part II

The above methods apply to periodic solutions of any period n. The case $n = 1$ corresponds to fixed points, discussed in §4. With $n = 2$, it suffices to consider $\mathcal{S} = LR$ for generic BCBs (refer to the discussion at the end of §6.2). Here we describe Feigin's analysis of LR-cycles [53, 55, 69, 70].

Let σ_J^- denote the number of real eigenvalues of A_J that are less than -1. If $I + A_J$ is nonsingular, then

$$\operatorname{sgn}\left(\det(I + A_J)\right) = (-1)^{\sigma_J^-} \,, \tag{6.13}$$

and we have the following result.

Proposition 6.5. *Suppose $\varrho^{\mathsf{T}} b \neq 0$, 1 is not an eigenvalue of $A_R A_L$, and -1 is not an eigenvalue of A_L or A_R. Then there exists a unique LR-cycle, and if $\sigma_L^- + \sigma_R^-$ is even [odd] then the LR-cycle is virtual for all $\mu \neq 0$ [admissible for exactly one sign of μ].*

In [53, 70] this result is proved directly. Here we provide a short proof by applying (6.9) to $\mathcal{S} = LR$.

Proof. An LR-cycle, $\{x_0^{LR}, x_1^{LR}\}$, is admissible if and only if $s_0^{LR} \leq 0$ and $s_1^{LR} \geq 0$. With $\mathcal{S} = LR$ we have $P_{\mathcal{S}} = I + A_R$ and $P_{\mathcal{S}^{(1)}} = I + A_L$, which are both nonsingular by assumption. In view of the remaining assumptions of Proposition 6.5, the right hand side of (6.9) is nonzero whenever $\mu \neq 0$. If $\sigma_L^- + \sigma_R^-$ is even, then by (6.13), $\det(P_{\mathcal{S}})$ and $\det(P_{\mathcal{S}^{(1)}})$ have the same sign, thus by (6.9), s_0^{LR} and s_1^{LR} have the same sign, hence the LR-cycle is virtual for all $\mu \neq 0$. If $\sigma_L^- + \sigma_R^-$ is odd, then s_0^{LR} and s_1^{LR} have different signs, and these depend on the sign of μ, hence the LR-cycle is admissible for exactly one sign of μ. □

From Propositions 4.1 and 6.5, and a little extra work, we can conclude that there are exactly four scenarios for the existence and relative coexistence of fixed points and period-two solutions near non-degenerate BCBs. These are illustrated in Table 1. To justify Table 1 we require the following two additional results. In these results $\sigma_{\mathcal{S}}^+$ denotes the number of real eigenvalues of $M_{\mathcal{S}}$ that are greater than 1.

Proposition 6.6. *Suppose $\varrho^{\mathsf{T}} b \neq 0$, 1 is not an eigenvalue of A_L, A_R or $A_R A_L$, -1 is not an eigenvalue of A_L or A_R, and $\sigma_L^- + \sigma_R^-$ is odd. If $\sigma_{LL}^+ + \sigma_{LR}^+$ is odd [even] then the LR-cycle coexists with x^L [does not coexist with x^L].*

For a proof of Proposition 6.6, refer to [52, 53, 70]. In the case that $\sigma_L^+ + \sigma_R^+$ is even and $\sigma_L^- + \sigma_R^-$ is odd, the even/odd parity of $\sigma_{LL}^+ + \sigma_{LR}^+$ determines which fixed point coexists with the LR-cycle. The next result is taken from [169].

Proposition 6.7. *Suppose 1 is not an eigenvalue of A_L, A_R or $A_R A_L$, and -1 is not an eigenvalue of A_L or A_R. If $\sigma_L^+ + \sigma_R^+$ and $\sigma_L^- + \sigma_R^-$ are odd, then $\sigma_{LL}^+ + \sigma_{LR}^+$ is also odd.*

If $\sigma_L^+ + \sigma_R^+$ and $\sigma_L^- + \sigma_R^-$ are both odd, then by Propositions 6.6 and 6.7 the LR-cycle coexists with both x^L and x^R rather than coexisting with neither x^L or x^R, as indicated in Table 1.

Table 1 constitutes a partial classification of BCBs. This classification does not appear to have a useful analogue for general PWL discontinuous maps, but has been extended to maps that differ from the form (1.4) only in that the constant parts of g^L and g^R are given by different vectors [66].

7 Attractors

Attractors created in BCBs can be chaotic. We expect that chaotic attractors involving transverse homoclinic connections are structurally stable, and so if such a chaotic attractor is present in the PWL approximation (1.4) with $\mu = 1$, then a similar chaotic attractor exists in (1.3) for small $\mu > 0$ [52]. However, this does not appear to have been demonstrated rigorously. As with other bounded invariant sets, chaotic attractors of (1.3) created at $\mu = 0$ will generically be of a size proportional to $|\mu|$, to leading order.

Chaotic attractors of (1.4) are often *robust* in the sense that if η is varied while $\mu \neq 0$ is held constant then a chaotic attractor can persist without windows of periodicity [21]. As detailed in [52], this is particularly evident for BCBs in one-dimension, see §11.1.

$\sigma_L^- + \sigma_R^-$ \ $\sigma_L^+ + \sigma_R^+$	even	odd
even	x^L and x^R admissible for different signs of μ; LR-cycle virtual for all $\mu \neq 0$	x^L and x^R admissible for the same sign of μ; LR-cycle virtual for all $\mu \neq 0$
odd	x^L and x^R admissible for different signs of μ; LR-cycle admissible for one sign of μ	x^L, x^R and the LR-cycle admissible for the same sign of μ

Table 1: A partial classification of BCBs. As discussed in §3, dynamics near a generic BCB are described by a PWL map of the form (1.4). As described in §4.2 and §6.6, σ_J^+ [σ_J^-] denotes the number of eigenvalues of A_J that are greater than 1 [less than -1]. The existence and relative coexistence of the fixed points x^L and x^R and of an LR-cycle near the BCB of (1.4) are determined by the even/odd parity of $\sigma_L^+ + \sigma_R^+$ and $\sigma_L^- + \sigma_R^-$, as indicated.

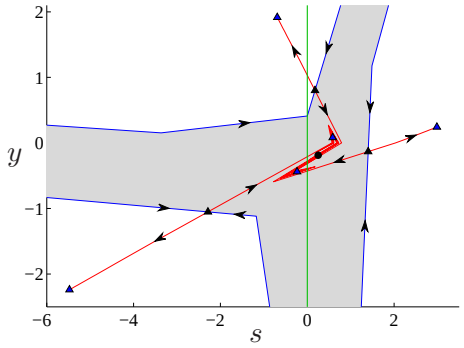

Figure 7: A phase portrait of (5.1) with (5.3), $x = (s, y)$, $(\tau_L, \delta_L, \tau_R, \delta_R) = (-0.1, 0.35, -2.25, 0.75)$ and $\mu = 1$. There is an attracting LR-cycle, an attracting LLR-cycle, a saddle-type LRR-cycle, and an unstable fixed point x^R. The basin of attraction of the LR-cycle (the shaded region) and the basin of attraction of the LLR-cycle (the unshaded region) are bounded by the stable manifold of the LRR-cycle.

7.1 Coexisting attractors

At a BCB it is possible that more than one attractor is created simultaneously. As an example, Fig. 7 shows a phase portrait of the PWL map (1.4) with $N = 2$, at parameter values for which there is an attracting LR-cycle and an attracting LLR-cycle for $\mu > 0$. For $\mu < 0$, the fixed point x^L is attracting (and appears to be a global attractor). As the value of μ is increased through zero, the LR-cycle and LLR-cycles are created simultaneously at the origin. From a practical viewpoint, the coexistence of attractors induces an inherent unpredictability in a neighbourhood of the BCB in the presence of noise, see §11.4.

With $N = 1$, coexisting attractors are not possible for (1.4), see §11.1. With $N \geq 2$, diverse types of attractors can coexist. For example with $N = 2$ (1.4) may have an attracting periodic solution and an attracting invariant circle [205], an attracting periodic solution and an apparently

chaotic attracting set [64], or several coexisting attractors [109] (see also §7.2). The following result is possibly the only known result regarding coexisting attractors of (1.4) that has no restriction on N:

Proposition 7.1. *For (1.4) with $\mu \neq 0$, there can be at most one attracting fixed point or period-two solution.*

This result follows simply from Feigin's classification outlined in §4.2 and §6.6. If the two fixed points x^L and x^R coexist, then by Proposition 4.1, $\sigma_L^+ + \sigma_R^+$ is odd, and thus by Proposition 6.4, x^L and x^R cannot both be attracting. With similar arguments, Proposition 6.5 can be used to show that if the LR-cycle is attracting, then any fixed point that coexists with the LR-cycle cannot also be attracting [52, 53, 70].

7.2 Extreme multistability

Large numbers of coexisting attractors have recently been identified for the two-dimensional border-collision normal form, (5.1) and (5.3), for which parameter space is four-dimensional (the parameters are τ_L, δ_L, τ_R and δ_R). Infinitely many attracting periodic solutions coexist at codimension-three points of parameter space that are characterised by the existence of a saddle-type periodic solution for which branches of its stable and unstable manifolds coincide [171]. Fig. 8 shows a phase portrait at parameter values extremely close to such a codimension-three point. At the codimension-three point, branches of the stable and unstable manifolds of an $RLLR$-cycle are coincident, and form an invariant hexagon that contains the basins of attraction of infinitely many periodic solutions.

At parameter values near such a codimension-three point, (5.1) exhibits a large number of attracting periodic solutions, say K. If ε denotes the distance in parameter space from the codimension-three point, then ε scales with λ^{-K}, where λ is the unstable stability multiplier of the relevant saddle-type periodic solution [170].

There also exist codimension-four points at which $M_{\mathcal{S}}$ has a repeated unit eigenvalue, for some symbol sequence $\mathcal{S}$, and (5.1) has infinitely many periodic solutions that are stable, but not attracting [170]. Despite the high codimension and lack of attraction, these points may be important because at nearby parameter values the periodic solutions can be attracting, and in this instance ε scales with K^{-2}. Therefore the number of attracting periodic solutions decays relatively slowly with distance, and so the codimension-four points influence relatively large regions of parameter space. It remains to extend these results to maps (1.4) of any number of dimensions.

7.3 Multi-dimensional attractors

In [95], Glendinning and Wong use Markov partitions to prove that chaotic two-dimensional attractors can be created in BCBs. Fig. 9 shows an example, taken from [95], of a PWL map of the form (1.4) for which typical forward orbits fill the interior of a quadrilateral, $\mathcal{R}$.

The division of $\mathcal{R}$ into eight closed regions $\mathcal{R}_j$, as shown, forms a *Markov partition* because

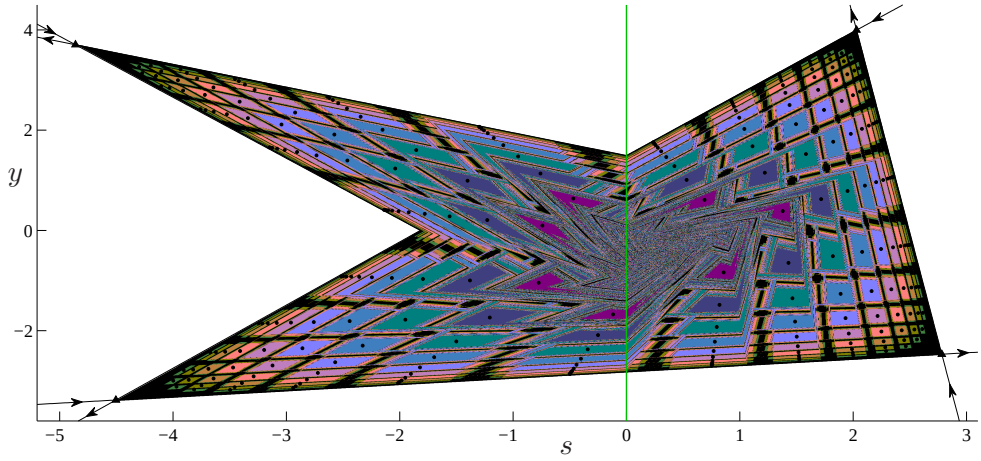

Figure 8: A phase portrait of (5.1) and (5.3), with $x = (s, y)$, $(\tau_L, \delta_L, \tau_R, \delta_R) = (0.55, \frac{1}{\delta_R}, -1.090903277, 1.216136849)$ and $\mu = 1$. These parameter values approximate (to ten significant figures) values at which (5.1) has an attracting $(RLLR)^k LLR$-cycle, for all $k \in \mathbb{Z}^+$. The first ten periodic solutions in this sequence are shown here (as black dots) and their basins of attraction are indicated by colour (from purple for $k = 1$, through to green for $k = 10$).

the image of each $\mathcal{R}_j$ under the map is a union of some of $\mathcal{R}_1, \ldots, \mathcal{R}_8$:

$$
\begin{aligned}
g(\mathcal{R}_1) &= \mathcal{R}_1 \cup \mathcal{R}_2 \,, & g(\mathcal{R}_2) &= \mathcal{R}_3 \cup \mathcal{R}_4 \,, \\
g(\mathcal{R}_3) &= \mathcal{R}_5 \,, & g(\mathcal{R}_4) &= \mathcal{R}_6 \,, \\
g(\mathcal{R}_5) &= \mathcal{R}_7 \,, & g(\mathcal{R}_6) &= \mathcal{R}_8 \,, \\
g(\mathcal{R}_7) &= \mathcal{R}_1 \cup \mathcal{R}_4 \cup \mathcal{R}_8 \,, & g(\mathcal{R}_8) &= \mathcal{R}_2 \cup \mathcal{R}_3 \,.
\end{aligned}
$$

With some additional assumptions, the existence of a Markov partition implies that (5.1) is *affine*

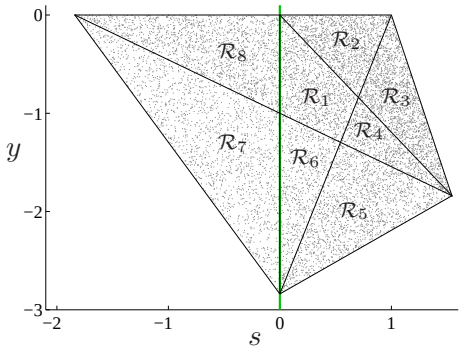

Figure 9: A phase portrait of the two-dimensional border-collision normal form, (5.1) and (5.3), with $x = (s, y)$, $\mu = 1$, and $(\tau_L, \delta_L, \tau_R, \delta_R) \approx (-0.2956, -1, 0.5437, 1.8393)$, specified exactly by $\tau_R^3 + \tau_R^2 + \tau_R - 1 = 0$, $\delta_R = \frac{1}{\tau_R}$, $\tau_L = -\tau_R^2$ and $\delta_L = -1$. The regions $\mathcal{R}_1 \ldots \mathcal{R}_8$ form a Markov partition of an invariant quadrilateral. Also shown are the points x_i, for $i = 5000, \ldots, 10000$, for the forward orbit of $x_0 = (-1, 0)$.

locally eventually onto on $\mathcal{R}$, from which we can say that (5.1) is chaotic on $\mathcal{R}$ [95]. Numerical results suggest that such attractors typically persist under parameter change [140].

Recently there have been efforts to extend these concepts to higher dimensions [92]. For example, with $\Delta_L = -2e_N$, $\Delta_R = 2e_N$ and $\mu = 1$, (5.1) is chaotic on the invariant hypercube $\mathcal{C} = [-1,1] \times [-2,0] \times \cdots \times [-2,0]$, although $\mathcal{C}$ is not an attractor. In this case the N^{th}-iterate of s_i is given simply by the tent map: $s_{i+N} = 1 - 2|s_i|$.

7.4 Attractors at infinity

Even though the PWL map (1.4) was constructed as an approximation to (1.3) at small values of x and μ, it is often useful to analyse the dynamics of (1.4) at infinity, i.e. on the *Poincaré sphere*, in order to obtain a deeper understanding of the BCB of (1.3) at $\mu = 0$. Dynamics on the Poincaré sphere can be explored via a compactification of phase space [137]. Under the coordinate change

$$z = \frac{x}{\sqrt{1 + \|x\|^2}} \,, \tag{7.1}$$

(1.4) is transformed to a PWS map on the N-dimensional unit ball, that we write as

$$z_{i+1} = \begin{cases} p^L(z_i;\mu,\eta) \,, & u_i \leq 0 \\ p^R(z_i;\mu,\eta) \,, & u_i \geq 0 \end{cases} \,, \tag{7.2}$$

where $u = e_1^{\mathsf{T}} z$. Expressions for p^L and p^R are relatively complicated, but on the boundary of the ball (7.2) is given simply by

$$z_{i+1} = \begin{cases} \frac{A_L z_i}{\|A_L z_i\|} \,, & u_i \leq 0 \\ \frac{A_R z_i}{\|A_R z_i\|} \,, & u_i \geq 0 \end{cases} \,, \qquad \|z_i\| = 1 \,. \tag{7.3}$$

The map (7.3) describes the dynamics of (1.4) on the Poincaré sphere. Notice that μ is absent from (7.3), thus the dynamics of (1.4) on the Poincaré sphere is independent of μ.

An $\mathcal{S}$-cycle of (7.3), denoted $\{z_i^{\mathcal{S}}\}$, is a periodic solution that follows the half-maps of (7.3) in the order determined by $\mathcal{S}$. Since the n^{th} iterate of (7.3) following $\mathcal{S}$ is given by $z_n = \frac{M_{\mathcal{S}} z_0}{\|M_{\mathcal{S}} z_0\|}$ (where $M_{\mathcal{S}}$ is the product (6.3)), $z_0^{\mathcal{S}}$ is an eigenvector of $M_{\mathcal{S}}$ with corresponding eigenvalue $\lambda = \|M_{\mathcal{S}} z_0^{\mathcal{S}}\| \neq 0$.

Evolution near $\{z_i^{\mathcal{S}}\}$ is governed by the Jacobian $\left(D_z p^{\mathcal{S}}\right)(z_0^{\mathcal{S}})$, and the stability of $\{z_i^{\mathcal{S}}\}$ is determined by the eigenvalues of this matrix. From an explicit expression for $\left(D_z p^{\mathcal{S}}\right)(z_0^{\mathcal{S}})$, we find that $\frac{1}{\lambda^2}$ is an eigenvalue of $\left(D_z p^{\mathcal{S}}\right)(z_0^{\mathcal{S}})$, with corresponding eigenvector $z_0^{\mathcal{S}}$. Moreover, if $\tilde{\lambda} \in \mathbb{R}$ is another eigenvalue of $M_{\mathcal{S}}$ ($\tilde{\lambda} \neq \lambda$), then $\frac{\tilde{\lambda}}{\lambda}$ is an eigenvalue of $\left(D_z p^{\mathcal{S}}\right)(z_0^{\mathcal{S}})$, and the corresponding eigenvector is equal to the projection of the eigenvector of $M_{\mathcal{S}}$ for $\tilde{\lambda}$ onto $\left(z_0^{\mathcal{S}}\right)^{\perp}$.

For example, the two-dimensional map illustrated in Fig. 10 has two $LLRLR$-cycles on the Poincaré sphere. For the given parameter values the eigenvalues of $M_{\mathcal{S}}$ with $\mathcal{S} = LLRLR$ are $\lambda_1 \approx 1.0430$ and $\lambda_2 \approx 0.7419$. With $\lambda = \lambda_1$ and $\tilde{\lambda} = \lambda_2$, we have $\left|\frac{1}{\lambda^2}\right|, \left|\frac{\tilde{\lambda}}{\lambda}\right| < 1$, hence the corresponding $\mathcal{S}$-cycle on the Poincaré sphere is attracting. With instead $\lambda = \lambda_2$ and $\tilde{\lambda} = \lambda_1$, we have $\left|\frac{1}{\lambda^2}\right|, \left|\frac{\tilde{\lambda}}{\lambda}\right| > 1$, hence the other $\mathcal{S}$-cycle on the Poincaré sphere is repelling.

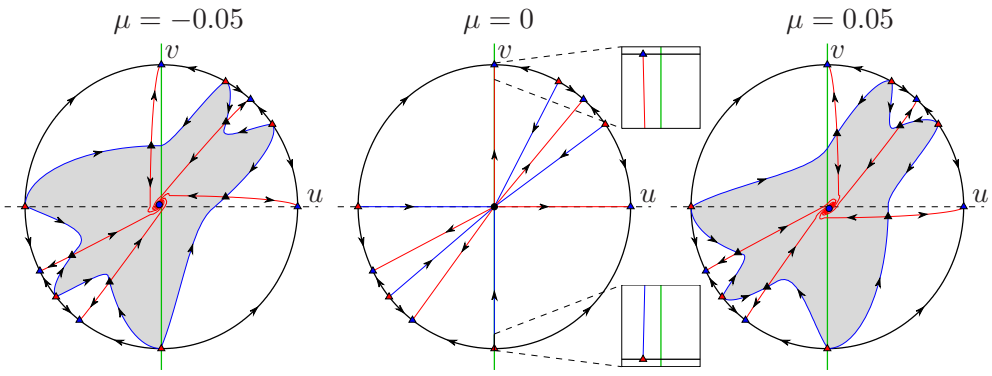

Figure 10: Phase portraits illustrating a dangerous bifurcation for the two-dimensional border-collision normal form, (5.1) and (5.3), with $(\tau_L, \delta_L, \tau_R, \delta_R) = (-1.33, 0.95, -1.87, 0.95)$, in compactified coordinates (7.1), where $z = (u, v)$. The circle bounding each plot corresponds to $\|z\| = 1$, and represents the Poincaré sphere of (5.1). In the left plot [right plot] there is a saddle-type $LLRLR$-cycle [$RLRLR$-cycle], and its stable and unstable manifolds are shown. In the left plot [right plot] the fixed point z^L [z^R] is attracting and the shaded region is its basin of attraction. The two $LLRLR$-cycles on the Poincaré sphere are independent of μ and each involve one point that is located just to the left of the switching manifold, as shown in the insets.

An $\mathcal{S}$-cycle of (1.4) undergoes a bifurcation at infinity when an eigenvalue of $M_{\mathcal{S}}$ attains the value 1 [15]. Except in special cases, at this bifurcation the $\mathcal{S}$-cycle of (1.4) collides with a second $\mathcal{S}$-cycle at infinity. The two $\mathcal{S}$-cycles interchange stability in a manner akin to a transcritical bifurcation and the $\mathcal{S}$-cycle of (1.4) becomes virtual, see §8.1.

7.5 Dangerous bifurcations

In the case that (1.4) has a unique fixed point for all $\mu \in \mathbb{R}$, it is possible for the fixed point to be attracting for all $\mu \neq 0$, yet unstable when $\mu = 0$. In this scenario the BCB is called a *dangerous bifurcation* [61, 62, 81, 100]. All eigenvalues of A_L and A_R have a modulus less than 1, so it may be surprising that $x = 0$ can be an unstable fixed point of (1.4) with $\mu = 0$ (although we require $N \geq 2$). The continuous-time analogue of this phenomenon requires at least three dimensions [32].

Ascertaining the stability of $x = 0$ for (1.4) with $\mu = 0$ is difficult, and the stability does not appear to relate to the eigenvalues of A_L and A_R in a simple manner. Due to the radial symmetry of (1.4) with $\mu = 0$, the distance of points from the origin can be scaled to 1, reducing (1.4) to a map on the unit sphere $\mathbb{S}^{N-1}$ together with a "dilation ratio" indicating the factor by which the distance from the origin changes under (1.4). It may be possible to determine the stability of the origin by evaluating dilation ratios over an invariant measure of the map on $\mathbb{S}^{N-1}$. To date this approach has only been explored for $N = 2$ [63].

A typical dangerous bifurcation is illustrated in Fig. 10, which is plotted in compactified coordinates (7.1). When $\mu = 0$ the origin is unstable because there is an attracting $LLRLR$-cycle on the Poincaré sphere. This attractor is independent of μ, hence are multiple attractors for all $\mu \neq 0$. The basin of attraction of the fixed point is bounded by the stable manifold of a

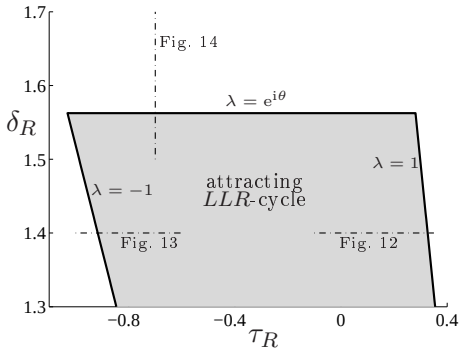

Figure 11: A two-parameter bifurcation diagram of the two-dimensional border-collision normal form, (5.1) and (5.3), with $\tau_L = -1.5$, $\delta_L = -0.8$ and $\mu > 0$. In the shaded region the map exhibits an attracting LLR-cycle. The LLR-cycle loses stability on the boundaries of this region via an associated stability multiplier λ (eigenvalue of M_{LLR}) crossing the unit circle as indicated. The dot-dashed line segments indicate the parameter values used in Figs. 12-14.

saddle-type $LLRLR$-cycle for $\mu < 0$, and a saddle-type $RLRLR$-cycle for $\mu > 0$. In compactified coordinates the area of the basin of attraction of the fixed point tends to zero as $\mu \to 0$. A three-dimensional example of a dangerous bifurcation is given in [42].

8 Loss of hyperbolicity for periodic solutions

As the additional parameter η is varied, the nature of the BCB of (1.3) at $\mu = 0$ can change. In this section we suppose that at a critical value of η, call it η^*, a non-hyperbolic $\mathcal{S}$-cycle is born in the BCB and exists for small $\mu > 0$. With $\eta = \eta^*$, $M_{\mathcal{S}}$ has an eigenvalue λ with $|\lambda| = 1$. There are three generic cases: $\lambda = 1$, $\lambda = -1$, and $\lambda = e^{i\theta}$ with $0 < \theta < \pi$. These constitute three different codimension-two BCBs, and each occurs for the example shown in Fig. 11.

The nature of the dynamics related to the non-hyperbolic $\mathcal{S}$-cycle is dependent on the nonlinear terms in f^L and f^R that were omitted to produce the PWL map (1.4). We start in §8.1 by looking at (1.4), then examine the effects of nonlinear terms with the example of Fig. 11. In §8.2 we formally describe unfoldings of the three codimension-two BCBs in the case that the $\mathcal{S}$-cycle is a fixed point, and speculate on unfoldings for general $\mathcal{S}$-cycles. Throughout this section it is assumed that $\det\left(P_{\mathcal{S}^{(i)}}\right) \neq 0$ for all i, so that the $\mathcal{S}$-cycle does not intersect the switching manifold for $\mu > 0$.

8.1 Loss of hyperbolicity in the piecewise-linear approximation

If $\lambda \to 1$ as $\eta \to \eta^*$ while $\mu > 0$ is held constant, then for (1.4) the $\mathcal{S}$-cycle grows in size without bound. This is shown in Fig. 12a for which τ_R takes the role of η. At $\eta = \eta^*$ the $\mathcal{S}$-cycle does not exist, but may be thought of as residing on the Poincaré sphere, see §7.4. In generic situations the sign of $\det(I - M_{\mathcal{S}})$ switches as we cross the bifurcation, in which case by (6.9) the $\mathcal{S}$-cycle becomes completely virtual (that is all points lie on the wrong side of $s = 0$ for admissibility).

As shown in Fig. 12, the inclusion of nonlinear terms can change the bifurcation at infinity

(panel a) into a saddle-node bifurcation (panel b). For this example, (1.3) is written as

$$x_{i+1} = \begin{cases} e_1\mu + C_L x_i + h^L(x_i)\,, & s_i \le 0 \\ e_1\mu + C_R x_i + h^R(x_i)\,, & s_i \ge 0 \end{cases}, \tag{8.1}$$

where h^L and h^R contain only nonlinear terms.

Now suppose $\lambda \to -1$ as $\eta \to \eta^*$, and first consider (1.4) with $\mu > 0$ at $\eta = \eta^*$. Let ζ denote an eigenvector of $M_{\mathcal{S}}$ corresponding to λ. For small $\varepsilon > 0$, the forward orbit of $x_0^{\mathcal{S}} + \varepsilon\zeta$ is an $\mathcal{S}^{[2]}$-cycle (that is, a period-doubled solution following $\mathcal{S}$). Generically there exists $\varepsilon_{\max} > 0$ such that for all $0 < \varepsilon < \varepsilon_{\max}$ the $\mathcal{S}^{[2]}$-cycle has no points on the switching manifold, and with $\varepsilon = \varepsilon_{\max}$ the $\mathcal{S}^{[2]}$-cycle has one point on the switching manifold, say $x_j^{\mathcal{S}^{[2]}}$. This "maximal" $\mathcal{S}^{[2]}$-cycle is therefore also an $\mathcal{S}^{[2]\overline{j}}$-cycle. Except in special cases, the $\mathcal{S}^{[2]\overline{j}}$-cycle is unique and admissible for values of η on one side of $\eta = \eta^*$. At $\eta = \eta^*$ an attracting $\mathcal{S}$-cycle can change to an attracting $\mathcal{S}^{[2]\overline{j}}$-cycle, in which case the bifurcation may be viewed as non-local period-doubling [168]. This phenomenon has also been described for discontinuous maps [11]. Alternatively an attracting $\mathcal{S}$-cycle can bifurcate to a $2n$-band chaotic attractor [131, 181], as in Fig. 13a (here $n = 3$).

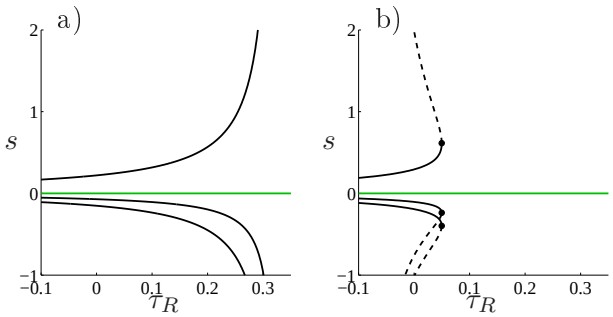

Figure 12: Panel a is a bifurcation diagram of (5.1) corresponding to a cross-section of Fig. 11 at $\delta_R = 1.4$ with $\mu = 0.05$. An attracting LLR-cycle loses stability at $\tau_R \approx 0.3266$ via an associated stability multiplier attaining the value 1. Panel b shows a corresponding bifurcation diagram of the PWS map (8.1) with $h^L = [s^2, 0]^\mathsf{T}$ and $h^R = [0, 0]^\mathsf{T}$.

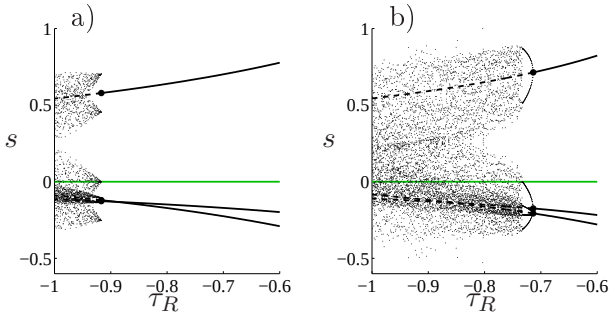

Figure 13: Panel a is a bifurcation diagram of (5.1) corresponding to a cross-section of Fig. 11 at $\delta_R = 1.4$ with $\mu = 0.5$. An attracting LLR-cycle loses stability at $\tau_R \approx -0.9167$ via an associated stability multiplier attaining the value -1. Panel b shows a corresponding bifurcation diagram of the PWS map (8.1) with $h^L = [s^2, 0]^\mathsf{T}$ and $h^R = [0, 0]^\mathsf{T}$.

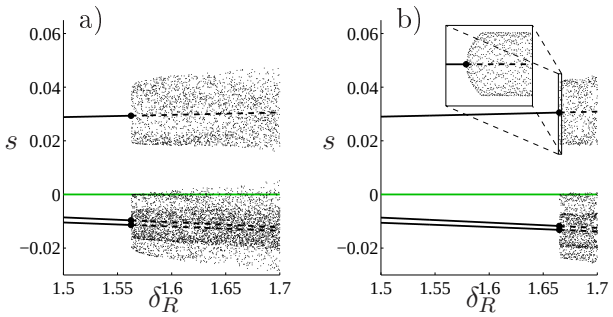

Figure 14: Panel a is a bifurcation diagram of (5.1) corresponding to a cross-section of Fig. 11 at $\tau_R = -0.7$ with $\mu = 0.02$. An attracting LLR-cycle loses stability at $\delta_R = 1.5625$ via an associated pair of complex stability multipliers attaining moduli of 1. Panel b shows a corresponding bifurcation diagram of the PWS map (8.1) with $h^L = [0, s^2]^\mathsf{T}$ and $h^R = [0, 0]^\mathsf{T}$.

In the presence of nonlinear terms, the $\lambda = -1$ bifurcation is generically a period-doubling (or flip) bifurcation at which a unique $\mathcal{S}^{[2]}$-cycle is created. Under further variation of η the $\mathcal{S}^{[2]}$-cycle undergoes a BCB, as in Fig. 13b.

Lastly, suppose $\lambda \to \mathrm{e}^{\mathrm{i}\theta}$, for some $0 < \theta < \pi$, as $\eta \to \eta^*$. This is shown for an example in Fig. 14a for which δ_R takes the role of η. If θ is irrational, then for (1.4) with $\mu > 0$, at $\eta = \eta^*$ there exists an uncountable nested collection of invariant sets that each consist of n disjoint ellipses centred at the points of the $\mathcal{S}$-cycle. Generically the largest set of n ellipses involves one point on the switching manifold. Alternatively if θ is rational, dynamics near the $\mathcal{S}$-cycle is periodic. The boundary of the periodicity regions may be a polygon, but this has only been described in detail in the case that the $\mathcal{S}$-cycle is a fixed point [80, 156, 172, 179].

In Fig. 14a, the $\mathcal{S}$-cycle is attracting prior to the $\lambda = \mathrm{e}^{\mathrm{i}\theta}$ bifurcation, and at the bifurcation the $\mathcal{S}$-cycle appears to change to a chaotic attractor. A similar bifurcation is described in [181]. If $\lambda = \mathrm{e}^{\mathrm{i}\theta}$ along a curve in parameter space, we expect that the value of θ varies along this curve. In this case Arnold tongues emanate from points on the curve at which θ is rational [168, 172, 179].

For the PWS map (1.3), the $\lambda = \mathrm{e}^{\mathrm{i}\theta}$ bifurcation generically corresponds to a Neimark-Sacker bifurcation at which an invariant circle is created about each point of the $\mathcal{S}$-cycle. The invariant circles grow until one of them collides with the switching manifold, Fig. 14b.

8.2 Unfoldings of non-hyperbolic fixed points

If (1.3) has a non-hyperbolic fixed point, say x^L, we can derive an unfolding of the codimension-two BCB by studying the extended centre manifold of f^L. This analysis only determines dynamics that are contained entirely within $s \leq 0$, but it is extremely general. For proofs of the theorems below, refer to [36, 168]. It remains to extend these results to $\mathcal{S}$-cycles of period $n > 1$. We expect that the essence of the unfoldings are unchanged with $n > 1$ because in principle the theorems given below can be applied to the n^{th} iterate of (1.3). However, there is some complexity in identifying the relevant iterate of the $\mathcal{S}$-cycle that interacts with the switching manifold.

Fig. 15 summarises the three unfoldings. In this figure, and for the remainder of this section, we assume $\eta \in \mathbb{R}$ and that each codimension-two BCB occurs at $(\mu, \eta) = (0, 0)$. Again we begin with the case $\lambda = 1$. In this case a locus of saddle-node bifurcations emanates from the

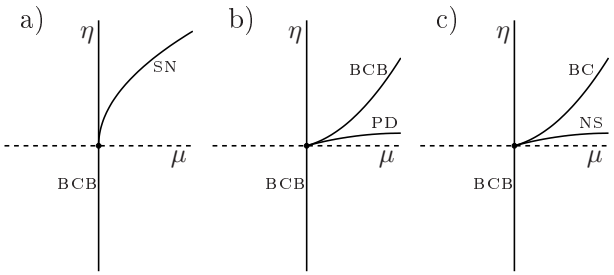

Figure 15: Unfoldings of codimension-two BCBs for which A_L has an eigenvalue λ with $|\lambda| = 1$ at $\eta = 0$. From left to right, the three unfoldings correspond to $\lambda = 1$, $\lambda = -1$, and $\lambda = \mathrm{e}^{\mathrm{i}\theta}$ with $0 < \theta < \pi$, as described in Theorems 8.1, 8.2 and 8.3 respectively. Loci of saddle-node, period-doubling and Neimark-Sacker bifurcations are denoted SN, PD and NS, respectively.

codimension-two point, tangent to $\eta = 0$, Fig. 15a. This is made precise by the following theorem.

Theorem 8.1. *Suppose (1.3) is piecewise-C^k ($k \geq 4$), $\lambda(\eta)$ is an eigenvalue of $A_L(\eta)$, and*

i) $\lambda(0) = 1$ *is of algebraic multiplicity* 1*, and $A_L(0)$ has no other eigenvalues of modulus* 1 *(eigenvalue condition);*

ii) $\varrho^{\mathsf{T}}(0)b(0) \neq 0$ *(genericity of BCB);*

iii) $\lambda'(0) \neq 0$ *(*transversality*).*

Then there exists a C^{k-1} extended centre manifold of f^L, $W^c(0;0,0)$, with the local representation $x = H(s;\mu,\eta)$. Let $F^L(s;\mu,\eta)$ denote the restriction of f^L to W^c and suppose

iv) $\frac{\partial^2 F^L}{\partial s^2}(0;0,0) \neq 0$ *(non-degeneracy of saddle-node bifurcation).*

Then for one sign of η (1.3) has a locus of saddle-node bifurcations $\mu = c_1\eta^2 + o(\eta^2)$, where $c_1 \neq 0$.

With instead $\lambda = -1$, a locus of period-doubling bifurcations emanates from the codimension-two point transverse to $\eta = 0$ (assuming non-degeneracy conditions are satisfied). An $L^{[2]}$-cycle (period-2 solution comprised of two points with $s \leq 0$) is created in the period-doubling bifurcation, and collides with the switching manifold along a curve that is tangent to the period-doubling locus, Fig. 15b. This bifurcation is a BCB, and the quadratic tangency is due to the fact that the distance of x^L from the switching manifold is proportional to μ, whereas the $L^{[2]}$-cycle grows at a rate proportional to the square root of the change in η from the period-doubling locus. On one side of the BCB of the $L^{[2]}$-cycle there exists an LR-cycle. If $N = 1$, a chaotic attracting set is created at the BCB of the $L^{[2]}$-cycle if and only if A_R (which in this case is a scalar) is greater than 1 [174]. In higher dimensions, numerical results suggest that for any $n \in \mathbb{Z}^+$, a 2^n-band chaotic attractor can be created at the BCB [181].

Theorem 8.2 formalises the unfolding shown in Fig. 15b. Prior to a proof of Theorem 8.2, the unfolding was observed numerically in a mathematical model of a DC/DC power converter [5, 6].

Theorem 8.2. *Suppose (1.3) is piecewise-C^k ($k \geq 4$), $\lambda(\eta)$ is an eigenvalue of $A_L(\eta)$, and*

i) $\lambda(0) = -1$ *is of algebraic multiplicity* 1*, and* $A_L(0)$ *has no other eigenvalues of modulus* 1 *(eigenvalue condition);*

ii) $\varrho^{\mathsf{T}}(0)b(0) \neq 0$ *(genericity of BCB);*

iii) $\lambda'(0) \neq 0$ *(transversality).*

iv) $e_1^{\mathsf{T}}\zeta(0) \neq 0$*, where* ζ *is the eigenvector of* A_L *corresponding to* λ *(centre manifold not tangent to switching manifold);*

v) $\det(I - A_L(0)A_R(0)) \neq 0$ *(genericity for existence of LR-cycle).*

Then there exists a C^{k-1} *extended centre manifold of* f^L*,* $W^c(0;0,0)$*, with the local representation* $x = H(s;\mu,\eta)$*. Let* $F^L(s;\mu,\eta)$ *denote the restriction of* f^L *to* W^c *and suppose*

vi) $\frac{1}{2}\left(\frac{\partial^2 F^L}{\partial s^2}(0;0,0)\right)^2 + \frac{1}{3}\frac{\partial^3 F^L}{\partial s^3}(0;0,0) \neq 0$ *(non-degeneracy of period-doubling bifurcation).*

Then for one sign of μ *(1.3) has a locus of period-doubling bifurcations at which an* $L^{[2]}$*-cycle is created,* $\eta = c_1\mu + c_2\mu^2 + o(\mu^2)$*, and a locus* $\eta = c_1\mu + c_3\mu^2 + o(\mu^2)$*, where* $c_3 \neq c_2$*, on which the* $L^{[2]}$*-cycle has a BCB.*

The final case $\lambda = \mathrm{e}^{\mathrm{i}\theta}$ exhibits a similar unfolding to the previous case. A locus of Neimark-Sacker bifurcations emanates transversally from the BCB locus, and along a tangent curve the bifurcating invariant circle intersects the switching manifold, Fig. 15c. Note that dynamics created by the collision of an invariant circle of (1.3) with a switching manifold do not appear to have been investigated in detail.

Theorem 8.3. *Suppose (1.3) is piecewise-*C^k *(*$k \geq 4$*),* $\lambda(\eta) = r(\eta)\mathrm{e}^{\mathrm{i}\theta(\eta)}$ *is an eigenvalue of* $A_L(\eta)$*, and*

i) $r(0) = 1$*,* $\lambda(0)$ *is of algebraic multiplicity* 1*, and* $A_L(0)$ *has no other eigenvalues of modulus* 1 *(eigenvalue condition);*

ii) $\mathrm{e}^{\mathrm{i}j\theta(0)} \neq 1$ *for* $j = 1,2,3,4$ *(not at strong resonance)*

iii) $\varrho^{\mathsf{T}}(0)b(0) \neq 0$ *(genericity of BCB);*

iv) $r'(0) \neq 0$ *(transversality).*

v) $e_1 \notin E^{\perp}$*, where* E *is the eigenspace of* $A_L(0)$ *corresponding to* $\lambda(0)$ *and* $\bar{\lambda}(0)$ *(centre manifold not tangent to switching manifold);*

Then there exists a C^{k-1} *extended centre manifold of* f^L*,* $W^c(0;0,0)$*, with the local representation* $x = H(s,y;\mu,\eta)$*, where* y *is a coordinate of* x *different to* s*. Let* $F^L(s,y;\mu,\eta)$ *denote the restriction of* f^L *to* W^c *and suppose*

vi) $\alpha \neq 0$ *for* F^L*, where* α *is the first Lyapunov exponent (non-degeneracy of Neimark-Sacker bifurcation).*

Then for one sign of μ *(1.3) has a locus of Neimark-Sacker bifurcations at which an invariant circle is created,* $\eta = c_1\mu + c_2\mu^2 + o(\mu^2)$*, and a locus* $\eta = c_1\mu + c_3\mu^2 + o(\mu^2)$*, where* $c_3 \neq c_2$*, on which the invariant circle grazes the switching manifold.*

9 Mode-locking regions

In this section we look at *mode-locking regions* of (1.3) and (1.4). These are regions of parameter space for which the map has an attracting periodic solution. In this context we treat $\mu \neq 0$ as fixed, and allow η to vary.

Fig. 16 illustrates mode-locking regions for a three-dimensional PWL map in border-collision normal form. Many of the regions exhibit a distinctive chain structure that loosely resembles a string of sausages. This structure is typical near BCBs and for PWL maps [172, 180, 207, 206], and has been described in models of power converters [204, 202, 209, 210], economics systems [80, 120, 156, 158, 182], dry friction oscillators [184], the human cardiorespiratory system [136], and in the integrate-and-fire neuron model (2.2) [186]. Instability regions of Hill's equation, $\ddot{x} + \big(a + b\,\mathrm{sgn}(\cos(t))\big)x = 0$, also exhibit this structure, but the instability regions are more spread out (because they are indexed by integers rather than an interval of rational numbers) [25, 189].

In order to explain the sausage structure, we first discuss bifurcations of (1.3) at which one point of an $\mathcal{S}$-cycle collides with the switching manifold under variation of η, §9.1. Most of the boundaries of the mode-locking regions in Fig. 16 correspond to such bifurcations. In contrast, for smooth systems boundaries of Arnold tongues correspond to saddle-node bifurcations [8, 115].

The sausage structure is related to the existence of invariant circles, and indeed mode-locking regions of sawtooth maps on $\mathbb{S}^1$ exhibit the same structure [30, 197]. However, rather than attempt to restrict the dynamics of (1.3) to an invariant circle, it is considerably simpler for us to instead restrict our attention to $\mathcal{S}$-cycles that, in a symbolic sense, correspond to rigid rotation on $\mathbb{S}^1$, §9.2. In §9.3 we unfold *shrinking points* – points where mode-locking regions have zero width – and use the result to explain the sausage structure.

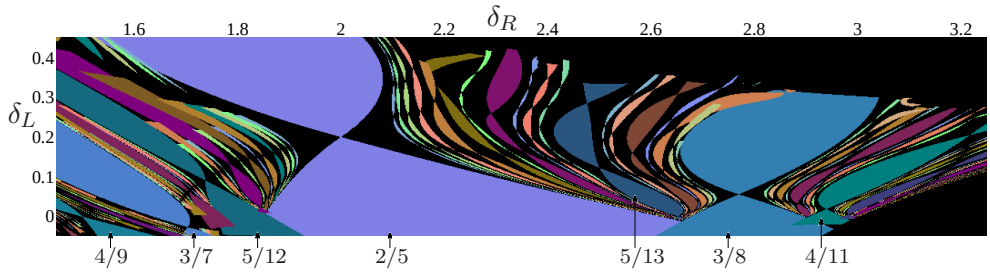

Figure 16: Mode-locking regions of (5.1) with $N = 3$, $\Delta_L = [0, -1, -\delta_L]^\mathsf{T}$, $\Delta_R = [2, 0, -\delta_R]^\mathsf{T}$, and $\mu = 1$. This figure was computed by explicitly calculating $\mathcal{S}$-cycles via (6.6) (up to period 50), and verifying stability and admissibility on a 1024×256 grid of parameter values. Different colours indicate different periods. Black indicates the absence of an attracting $\mathcal{S}$-cycle of period $n \leq 50$. The mode-locking regions of this figure correspond to $\mathcal{S}$-cycles that are "rotational", as defined in §9.2, and the largest mode-locking regions are labelled by their corresponding rotation number m/n (n is the period). The value of m/n roughly decreases from left to right across the figure. Some mode-locking regions overlap, in which case the colour corresponding to the higher period is used.

9.1 Border-collision bifurcations of periodic solutions

Suppose that under variation of η with $\mu \neq 0$ fixed, one point of an $\mathcal{S}$-cycle of (1.3) collides with the switching manifold. This corresponds to the BCB of a fixed point of the n^{th} iterate of (1.3), and local dynamics are described by a map of the form (1.3). This is made explicit by Theorem 9.1. In Theorem 9.1 we assume (without loss of generality) that it is the point $x_0^{\mathcal{S}}$, of the $\mathcal{S}$-cycle, that intersects the switching manifold, and $\mathcal{S}_0 = L$. For simplicity we also assume $\eta \in \mathbb{R}$. In Theorem 9.1 the BCB of the $\mathcal{S}$-cycle occurs at $\eta = h(\mu)$ for $\mu > 0$. We omit a proof of Theorem 9.1 which can be achieved by using the implicit function theorem to construct h.

Theorem 9.1. *Suppose (1.3) is piecewise-C^k ($k \geq 2$), $\mathcal{S}$ is a periodic symbol sequence of period n with $\mathcal{S}_0 = L$, and*

i) $\varrho^{\mathsf{T}}(0)b(0) \neq 0$;

ii) $\det(P_{\mathcal{S}}(0)) = 0$;

iii) $\frac{d\det(P_{\mathcal{S}})}{d\eta}(0) \neq 0$;

iv) with $\mu > 0$ and $\eta = 0$, the PWL approximation (1.4) has a unique admissible $\mathcal{S}$-cycle with exactly one point on the switching manifold ($x_0^{\mathcal{S}}$).

Then there exists a unique C^{k-1} function h, with $h(0) = 0$, such that $s_0^{\mathcal{S}}(\mu, h(\mu)) = 0$, for small $\mu \in \mathbb{R}$. Let

$$\hat{x} = x - x_0^{\mathcal{S}}(\mu, h(\mu)) \,, \qquad \hat{\eta} = \eta - h(\mu) \,. \tag{9.1}$$

Then, locally, the n^{th} iterate of (1.3) is given by

$$\hat{x}_n = \begin{cases} c(\mu)\mu\hat{\eta} + (M_{\mathcal{S}}(0) + O(\mu))\,\hat{x}_0 + o\left(\|\hat{x}_0\|, \hat{\eta}\right) \,, & \hat{s}_0 \leq 0 \\ c(\mu)\mu\hat{\eta} + (M_{\mathcal{S}^{\overline{0}}}(0) + O(\mu))\,\hat{x}_0 + o\left(\|\hat{x}_0\|, \hat{\eta}\right) \,, & \hat{s}_0 \geq 0 \end{cases} , \tag{9.2}$$

where $c : \mathbb{R} \to \mathbb{R}^N$ is C^{k-2} and $e_1^{\mathsf{T}}\text{adj}(I - M_{\mathcal{S}}(0))c(0) \neq 0$.

Since (9.2) is of the form (1.3), we can apply the results of earlier sections to investigate the dynamics created in the bifurcation $\eta = h(\mu)$. For instance, we can classify the BCB using Table 1. Here fixed points and period-two solutions of (9.2) correspond to $\mathcal{S}$-cycles, $\mathcal{S}^{\overline{0}}$-cycles, and $\mathcal{S}^{[2]\overline{0}}$-cycles of (1.3).

It is instructive to apply Theorem 9.1 to the border-collision normal form (5.1). Since (5.1) has $2N$ parameters and BCBs are codimension-one, given a periodic symbol sequence $\mathcal{S}$ and the index of the point undergoing border-collision, only a codimension-one subset of all BCBs are possible for (9.2). General properties of these codimension-one subsets are not known, but certainly diverse dynamics can be created in BCBs of (9.2).

If a periodic solution is created in the BCB of (9.2) at $\eta = h(\mu)$, it is possible that this periodic solution undergoes a BCB as another parameter is varied. This suggests that we could apply Theorem 9.1 several times. However, this does not appear to be useful because at each step we add one codimension. *Leonov's method* is a similar nesting concept for obtaining explicit expressions for parameter values at which periodic solutions of one-dimensional discontinuous maps undergo border-collision [14, 85, 125]. In this method the parameter values of the bifurcation

are determined from those of periodic solutions of one less *complexity level*. It is not possible to usefully apply Leonov's method to (1.3) without an explicit expression capturing the step from one complexity level to the next. Such an expression appears to be unavailable for (1.3) with $N > 1$.

Finally, it is not helpful to apply Theorem 9.1 to an $\mathcal{S}$-cycle with $n < 3$. This is because with $n = 1$, the $\mathcal{S}$-cycle is a fixed point and cannot intersect the switching manifold of (1.4) for $\mu \neq 0$ while the non-degeneracy condition $\varrho^{\mathsf{T}} b \neq 0$ is satisfied, see §4.3. If an LR-cycle of (1.4) has one point on the switching manifold for $\mu \neq 0$ and $\varrho^{\mathsf{T}} b \neq 0$, then one of the fixed points of (1.4) must have an associated eigenvalue of -1. For this reason it is more useful to treat the bifurcation as the loss of hyperbolicity of a fixed point, as in §8.1.

9.2 Rotational symbol sequences

Let $\ell, m, n \in \mathbb{Z}^+$, with $\ell < n$, $m < n$ and $\gcd(m, n) = 1$ (i.e. m and n are coprime). Let $\mathcal{S}[\ell, m, n] : \mathbb{Z} \to \{L, R\}$ be the period-n symbol sequence defined by

$$\mathcal{S}[\ell, m, n]_i = \begin{cases} L\,, & im \bmod n < \ell \\ R\,, & im \bmod n \geq \ell \end{cases} . \tag{9.3}$$

As in [173, 175], we refer to a sequence (9.3), and any cyclic permutation of (9.3), as *rotational*. Note that $\mathcal{S}[\ell, m, n]_0 = L$, and the number of L's per period is ℓ. For example $\mathcal{S}[4, 3, 8] = LLRLRRLR$, where, as described in §6.1, to state $\mathcal{S}$ we list the symbols $\mathcal{S}_0 \cdots \mathcal{S}_{n-1}$.

$\mathcal{S}[\ell, m, n]$ corresponds to rigid rotation of rotation number m/n on $\mathbb{S}^1$, where $[0, \ell/n) \subset \mathbb{S}^1$ is identified with the symbol L, and the remaining part of $\mathbb{S}^1$ is identified with the symbol R. For this reason, if (1.3) has an invariant circle that intersects the switching manifold at two points, and the restriction of (1.3) to this circle is a monotone increasing circle map, then the symbol sequence of any $\mathcal{S}$-cycle of (1.3) contained on the invariant circle is rotational. Consequently we refer to m/n as the *rotation number* of $\mathcal{S}[\ell, m, n]$.

Rotational symbol sequences appear to have been first studied by Slater [176, 177] who proved the "three gap theorem" [3]. In the context of (9.3), this theorem states that for any $\mathcal{S}[\ell, m, n]$, there are at most three values for the number of steps between consecutive instances of the symbol L, and if there are three distinct values then the largest value is the sum of the other two. For example, $\mathcal{S}[4, 3, 8] = LLRLRRLR$ and the number of steps from the first L to the second L is 1, from the second L to the third L is 2, and from the third L to the fourth L is 3. By symmetry the statement remains true when L is replaced by R. Rotational symbol sequences were studied for circle maps in [167], and applied to a cardiac model in [40]. They are similar to Sturmian sequences (also called rotation sequences) which correspond to an irrational rotation number [75, 144, 190, 191].

9.3 Shrinking points

Points at which mode-locking regions have zero width are referred to as *shrinking points*. Fig. 17 illustrates dynamics near one shrinking point of Fig. 16. Several useful statements can be proved about mode-locking regions near shrinking points by assuming that the related symbol sequences are rotational. We can then obtain a qualitative description of the global structure of the mode-locking regions by extrapolating from shrinking points and assuming no other bifurcations occur.

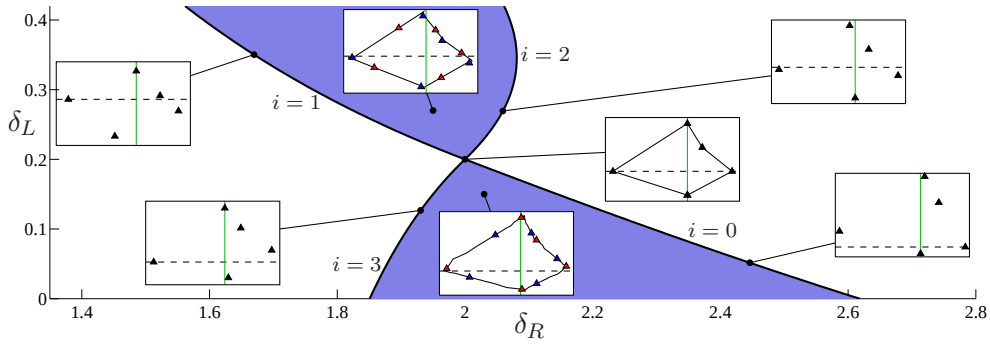

Figure 17: A plot of the mode-locking region with $m/n = 2/5$ of Fig. 16, centred at the shrinking point corresponding to $\mathcal{S}[2, 2, 5] = LRRLR$. The boundaries of the mode-locking region correspond to $\det(P_{\mathcal{S}^{(i)}}) = 0$, for $i = 0, \ldots, 3$, at which the i^{th} point of an $\mathcal{S}[2, 2, 5]$-cycle lies on the switching manifold. Insets show periodic solutions in (s, y)-coordinates, where s and y denote the first and second components of $x \in \mathbb{R}^3$. Inside the mode-locking region, the unstable manifold of the saddle-type periodic solution forms an invariant circle.

The mode-locking regions of Fig. 16 all correspond to rotational symbol sequences, and although periodic solutions with non-rotational symbol sequences can be created in border-collision bifurcations, they appear to be less common and not conducive to the sausage structure [168].

Each shrinking point is associated with a particular rotational symbol sequence, $\mathcal{S}[\ell, m, n]$. For example, in Fig. 17, $[\ell, m, n] = [2, 2, 5]$. On one side of the shrinking point there exist $\mathcal{S}[\ell, m, n]$ and $\mathcal{S}[\ell - 1, m, n]$-cycles, and on the other side of the shrinking point there exist $\mathcal{S}[\ell, m, n]$ and $\mathcal{S}[\ell + 1, m, n]$-cycles. On one side of the shrinking point the $\mathcal{S}[\ell, m, n]$-cycle is attracting, and on the other side of the shrinking point either the $\mathcal{S}[\ell - 1, m, n]$-cycle or the $\mathcal{S}[\ell + 1, m, n]$-cycle is attracting. Consequently, mode-locking regions correspond to attracting periodic solutions with rotational symbol sequences for which the value of l changes by one each time we cross a shrinking point. Throughout a mode-locking region, the rotation number m/n is constant. As with Arnold tongues of smooth systems [7, 8, 138], the mode-locking regions are roughly ordered by the rotation number m/n, and their overall width decreases with increasing n. Additional bifurcations apparent in Fig. 16 correspond to stability loss of the periodic solutions.

Boundaries of mode-locking regions near shrinking points are BCBs of nonsmooth fold type, at which the two coexisting periodic solutions coincide and have one point on the switching manifold. Let d denote the multiplicative inverse of m modulo n. It can be shown from (9.3) that the coincidence of an $\mathcal{S}[\ell, m, n]$-cycle and an $\mathcal{S}[\ell - 1, m, n]$-cycle by there being one point on the switching manifold is an $\mathcal{S}[\ell, m, n]$-cycle for which either $x_0^{\mathcal{S}}$ or $x_{(\ell-1)d \bmod n}^{\mathcal{S}}$ lies on the switching manifold. The coincidence of an $\mathcal{S}[\ell, m, n]$-cycle and an $\mathcal{S}[\ell+1, m, n]$-cycle, is similarly an $\mathcal{S}[\ell, m, n]$-cycle for which either $x_{\ell d}^{\mathcal{S}}$ or $x_{-d}^{\mathcal{S}}$ lies on the switching manifold, where here and for the remainder of this section we omit the "mod n" for brevity. For this reason, near the shrinking point the mode-locking region is bounded by the curves $\det(P_{\mathcal{S}^{(i)}}) = 0$, for $i = 0$, $(\ell - 1)d$, ℓd, and $-d$.

The $\mathcal{S}[\ell - 1, m, n]$ and $\mathcal{S}[\ell + 1, m, n]$-cycles coincide at the shrinking point. Let $\tilde{x}_i$ denote the points of this periodic solution, for which

$$\tilde{s}_0 = 0 \,, \qquad \tilde{s}_{\ell d} = 0 \,. \tag{9.4}$$

In view of (9.4), both $\tilde{x}_0$ and $\tilde{x}_d$ may be treated as the 0^{th}-point of an admissible $\mathcal{S}[\ell,m,n]$-cycle. Consequently, every point on the line segment connecting $\tilde{x}_0$ to $\tilde{x}_d$ belongs to an $\mathcal{S}[\ell,m,n]$-cycle, and the union of all of these $\mathcal{S}[\ell,m,n]$-cycles is an invariant circle in the form of a non-planar polygon [173]. Since the $\mathcal{S}[\ell,m,n]$-cycles are non-unique, by Propositions 6.1 and 6.2 we must have $\det(I - M_{\mathcal{S}[\ell,m,n]}) = 0$ and $\det\left(P_{\mathcal{S}[\ell,m,n]^{(i)}}\right) = 0$, for all i.

Also, as shown in [175], the periodic solution $\{\tilde{x}_i\}$ satisfies

$$\frac{\tilde{s}_d \tilde{s}_{(\ell-1)d}}{\tilde{s}_{-d}\tilde{s}_{(\ell+1)d}} = -\frac{\det\left(I - M_{\mathcal{S}[\ell-1,m,n]}\right)}{\det\left(I - M_{\mathcal{S}[\ell+1,m,n]}\right)} \,. \tag{9.5}$$

Here we verify (9.5) for an example. Consider the map (5.1) with $N = 3$, $\mu = 1$, and

$$\Delta_L = \begin{bmatrix} 0 \\ -1 \\ -\frac{\delta_R+2}{\delta_R\left(\delta_R^2+2\delta_R+2\right)} \end{bmatrix} \,, \qquad \Delta_R = \begin{bmatrix} \frac{\delta_R^2+\delta_R+2}{\delta_R+2} \\ 0 \\ -\delta_R \end{bmatrix} \,. \tag{9.6}$$

For all $\delta_R > 0.5865$, approximately, (5.1) with (9.6) has a shrinking point with $\mathcal{S}[2,2,5]$. The shrinking point shown in Fig. 17 corresponds to this map with $\delta_R = 2$. From direct calculations of (5.1) with (9.6) we obtain

$$\det\left(I - M_{\mathcal{S}[1,2,5]}\right) = -\frac{\phi(\delta_R)}{\delta_R(\delta_R+2)^3\left(\delta_R^2+2\delta_R+2\right)} \,, \tag{9.7}$$

$$\det\left(I - M_{\mathcal{S}[3,2,5]}\right) = \frac{(\delta_R+1)\phi(\delta_R)}{\delta_R^3(\delta_R+2)\left(\delta_R^2+2\delta_R+2\right)^3} \,, \tag{9.8}$$

where $\phi(\delta_R)$ is a particular eighth-order polynomial. Also, $\tilde{x}_0 = (0,-1,\delta_R)$, from which the other points $\tilde{x}_i$ can be computed by simply iterating this point under (5.1), and from which we find that both sides of (9.5) are given by $\frac{\delta_R^2\left(\delta_R^2+2\delta_R+2\right)^2}{(\delta_R+2)^2(\delta_R+1)}$.

Next we look at an unfolding of an arbitrary shrinking point for the PWL map (1.4). In the following theorem, taken from [173], we suppose for simplicity that $\eta \in \mathbb{R}^2$, the shrinking point is at $\eta = (0,0)$, and that we can choose coordinates $\eta = (\eta_1,\eta_2)$, such that

$$\begin{aligned} \det(P_{\mathcal{S}}(0,\eta_2)) &= 0 \,, \\ \det\left(P_{\mathcal{S}^{(\ell-1)d}}(\eta_1,0)\right) &= 0 \,, \end{aligned} \tag{9.9}$$

in a neighbourhood of $\eta = (0,0)$.

Theorem 9.2. *Suppose (1.4) is piecewise-C^k ($k \geq 3$), we have (9.9) for some $\mathcal{S}[\ell,m,n]$ with $2 \leq \ell \leq n-2$, and*

i) $\varrho^{\mathsf{T}}(0)b(0) \neq 0$;

ii) $\det(I - M_{\mathcal{S}[\ell-1,m,n]}(0)) \neq 0$ *and* $\det(I - M_{\mathcal{S}[\ell+1,m,n]}(0)) \neq 0$.

Then there exist unique C^{k-1} functions

$$\phi_1(\eta_1) = -c_1\eta_1^2 + o\left(\eta_1^2\right) \,, \qquad \phi_2(\eta_2) = -c_2\eta_2^2 + o\left(\eta_2^2\right) \,, \tag{9.10}$$

with $c_1, c_2 > 0$*, such that*

$$\begin{aligned} \det\left(P_{\mathcal{S}^{(-d)}}\left(\eta_1, \phi_1(\eta_1)\right)\right) &= 0 \,, \\ \det\left(P_{\mathcal{S}^{(1d)}}\left(\phi_2(\eta_2), \eta_2\right)\right) &= 0 \,, \end{aligned} \tag{9.11}$$

in a neighbourhood of $\eta = (0, 0)$*.*

Theorem 9.2 explains the local structure shown in Fig. 17. The four BCB curves that bound the mode-locking region are pairwise tangent at the shrinking point. The inequalities $c_1, c_2 > 0$ imply that as we move away from the shrinking point the left and right boundaries of the mode-locking region curve towards one another, relative to the curvature of the boundaries on the other side of the shrinking point. This curvature favours the boundaries reconnecting at another shrinking point, and thus forming the global sausage structure.

The dynamics associated with shrinking points is structurally unstable. Indeed typical mode-locking regions of (1.3) with small $\mu \neq 0$ exhibit the overall sausage structure, but have nonzero width in areas near where the PWL approximation to (1.3) has shrinking points [175]. Numerical investigations have revealed that nearby shrinking points have similar properties, but this has not been explained quantitatively. Loci of shrinking points sometimes appear to form a boundary for chaotic dynamics [172], and it remains to identify the precise mechanism responsible for the creation, or termination, of chaos in this manner. The invariant polygons that exist at shrinking points may persist as invariant circles (discussed in the next section) for nearby parameter values.

10 Other dynamics

10.1 Invariant circles

As noted in §2.4, an invariant circle appears to be created at the BCB shown in Fig. 3b. This BCB may therefore be viewed as a nonsmooth analogue of a Neimark-Sacker bifurcation [172, 203]. Except in special cases (such as shrinking points, §9.3) explicit expressions for invariant circles created in BCBs are not available. Indeed invariant circles created in BCBs often have an irregular shape. For this reason it does not appear to be possible to derive a circle map describing dynamics on the invariant circle by restricting (1.3) to the invariant circle in an explicit manner.

Numerical explorations have revealed that if an invariant circle is created in the BCB of (1.3) at $\mu = 0$ for some value of η, then the invariant circle typically persists as η is varied. We cannot immediately use normal hyperbolicity [71, 101, 160] to prove the persistence of an invariant circle, because (1.3) is not differentiable on the switching manifold. As described in [179, 208], invariant circles for (1.3) can be destroyed via mechanisms that occur for smooth maps [1, 9], such as due to a change in the stability of a periodic solution on the invariant circle. For invariant circles of (1.3) containing two periodic solutions whose symbolic representations differ by one symbol, as is common throughout mode-locking regions, the invariant circle can be destroyed in a BCB of the two periodic solutions [179]. In the case that (1.3) is non-invertible, an invariant circle can be destroyed by colliding with a critical surface (where the range of (1.3) has a fold) [79]. As discussed in the next section, invariant circles can also be destroyed in homoclinic bifurcations.

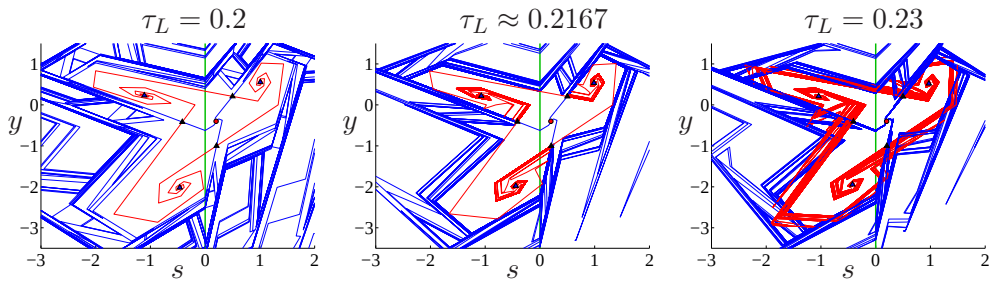

Figure 18: Phase portraits of (5.1) and (5.3) with $x = (s, y)$, $\mu = 1$, $\delta_L = 0.5$, $\tau_R = -2$, $\delta_R = 2$, and three different values of τ_L, as indicated. In each plot, the fixed point x^R is repelling, and there exists an attracting LLR-cycle and a saddle-type LRR-cycle. The stable and unstable manifolds of the LRR-cycle are coloured blue and red, respectively. In the middle plot the LRR-cycle has a homoclinic corner.

10.2 Homoclinic bifurcations

Consider a saddle-type $\mathcal{S}$-cycle of the PWL map (1.4). If the $\mathcal{S}$-cycle has no points on the switching manifold, then the stable and unstable manifolds emanate linearly from the $\mathcal{S}$-cycle in the directions of the stable and unstable eigenspaces of $M_{\mathcal{S}^{(i)}}$. Globally the invariant manifolds are PWL, due to interactions with the switching manifold. This property can be exploited to numerically compute invariant manifolds quickly and accurately. For instance, the one-dimensional invariant manifolds of Fig. 18 were computed via an iterated procedure of identifying points at which the invariant manifolds intersect the switching manifold, computing images of the intersection points, and appropriately connecting the points with line segments.

If the stable and unstable manifolds of an $\mathcal{S}$-cycle develop an intersection under parameter change, then an orbit homoclinic to the $\mathcal{S}$-cycle is created. For smooth maps, this constitutes a *first homoclinic tangency* at which the intersections of the stable and unstable manifolds are tangential [152]. For the PWL map (1.4), however, near each intersection one manifold is linear and the other manifold has a corner. For this reason we refer to this phenomenon as a *homoclinic corner*. Beyond the homoclinic corner, the stable and unstable manifolds intersect transversally, implying the existence of topological horseshoes and chaotic dynamics.

Fig. 18 shows an example in two dimensions. An LRR-cycle develops homoclinic connections as the parameter τ_L is increased. It is interesting that since the manifolds are PWL, linear pieces of the manifolds emanating from the LRR-cycle can be computed analytically, from which it can be shown that the homoclinic corner occurs at a root of $128\tau_L^8 + 896\tau_L^7 + 2488\tau_L^6 + 3292\tau_L^5 + 1729\tau_L^4 - 328\tau_L^3 - 566\tau_L^2 - 45\tau_L + 34 = 0$. This is an example of the general observation that various calculations that are intractable for smooth maps can be achieved exactly for PWL maps.

For a smooth map, an infinite sequence of "single-round" periodic solutions exists near a generic homoclinic tangency [86, 87, 88]. Such periodic solutions consist of a large number of points near the underlying saddle-type periodic solution, and one excursion far from the saddle-type solution. If the saddle-type solution is more strongly attracting than repelling, then there exists an infinite sequence of non-overlapping intervals of parameter values, bounded by saddle-node and period-doubling bifurcations, within which a single-round periodic solution exists and is attracting.

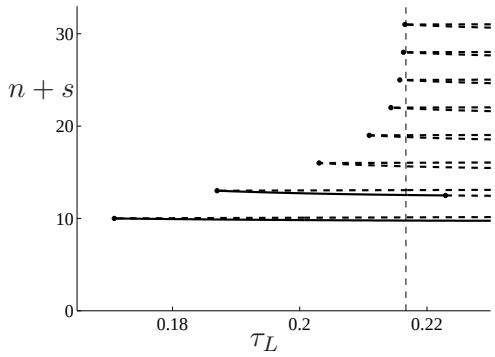

Figure 19: A bifurcation diagram of the two-dimensional PWL map of Fig. 18, indicating $\mathcal{S}[k]$ and $\mathcal{S}[k]^{\overline{0}}$-cycles, where $\mathcal{S}[k] = LRLLRLL\,(RRL)^k$, for $k = 1, \ldots, 8$. These are single-round periodic solutions associated with a saddle-type LRR-cycle. On the vertical axis we have plotted $n(k) + s_0^{\mathcal{S}[k]}$, where $n(k) = 3k+7$ is the period of the $\mathcal{S}[k]$-cycle and $s_0^{\mathcal{S}[k]}$ is the first component of the 0^{th}-point of the $\mathcal{S}[k]$-cycle (and similarly $n(k) + s_0^{\mathcal{S}[k]^{\overline{0}}}$ is plotted for the $\mathcal{S}[k]^{\overline{0}}$-cycles). These quantities are indicated with a solid [dashed] line if the periodic solution is stable [unstable].

In contrast, near the homoclinic corner of Fig. 18 there exists an infinite sequence of BCBs at which single-round periodic solutions are created, Fig. 19. The periodic solutions created in the BCBs are unstable (except for the first two BCBs in the sequence). By comparing this bifurcation diagram to those near homoclinic tangencies of smooth maps, it appears that each BCB can be interpreted as a nonsmooth amalgamation of saddle-node and period-doubling bifurcations. This suggests that an infinite sequence of intervals within which single-round periodic solutions are attracting does not arise near homoclinic corners. A general study of homoclinic corners remains for future work.

Other aspects of homoclinic corners have been described numerically in nonsmooth mathematical models for which they are relatively dominant bifurcations. Numerical-based studies have revealed that at a homoclinic corner an invariant circle can be destroyed [206, 207], or a chaotic attractor can be created [206]. In addition, if the stable manifold of the saddle-type periodic solution is a boundary of a basin of attraction of a chaotic attractor, the number of bands in the attractor may change at the homoclinic corner [131].

10.3 Consequences of a lack of invertibility

As explained in §3.4, if $\det(A_L)\det(A_R) \leq 0$, then (1.4) is non-invertible. In this case the image of the switching manifold is a boundary for the range of (1.4), and is referred as a *critical manifold*. If $\det(A_L)\det(A_R) < 0$, then points on one side of the critical manifold have two preimages and points on the other side of the critical manifold have no preimages.

The collision of an invariant set of a non-invertible map with a critical manifold is known as *contact bifurcation*, and often corresponds to a global bifurcation [140]. For instance if a basin of attraction is comprised of several disjoint sets, then the number of sets may change when the basin collides with a critical manifold. A wide variety of contact bifurcations are described for maps of the form (1.4) in [83, 140, 141]. For (1.4), a contact bifurcation is equivalent to a

border-collision (i.e. the collision of an invariant set with the switching manifold).

A repelling fixed point, call it x, has no local stable manifold, yet for a non-invertible map it is possible that a sequence of preimages of x tends to x, in which case x has a homoclinic orbit. Under some technical assumptions, x is in this case called a *snap-back repeller*, and its existence implies the presence of an unstable chaotic set, as well as infinitely many unstable periodic solutions [134, 135, 164]. These unstable periodic solutions can themselves have homoclinic orbits, and for this reason snap-back repellers are associated with a complicated bifurcation structure akin to that of homoclinic tangles [90]. Snap-back repellers are possible for (1.4) [94], and thus can be created at BCBs.

11 Special cases and generalisations

11.1 The one-dimensional case

In one-dimension, (1.4) is a skew tent map which we write as

$$x_{i+1} = \begin{cases} a_L x_i + \mu \,, & x_i \leq 0 \\ a_R x_i + \mu \,, & x_i \geq 0 \end{cases} \,. \tag{11.1}$$

Here $x = s$ and the magnitude of μ has been scaled to absorb b. Equation (11.1), and other one-dimensional PWS continuous maps, have been studied by various authors in diverse contexts [18, 53, 70, 110, 132, 149, 181].

For any choice of parameter values, (11.1) has non-positive *Schwarzian derivative* on $\mathbb{R}\backslash\{0\}$, and thus has at most one attractor [128, 139]. Fig. 20 indicates the attractor of (11.1) for $\mu > 0$ and different values of a_L and a_R. For values of a_L and a_R in regions labelled $L^{n-1}R$, for $n \geq 1$, there exists an attracting $L^{n-1}R$-cycle. With a_L fixed at 0.25, say, by decreasing the value of a_R we produce a *period incrementing cascade*: windows of periodicity for which the period increases by one from each window to the next [13, 34, 99]. Note that a nonlinear scale is used on the vertical axis of Fig. 20 so that many of the mode-locking regions can be seen.

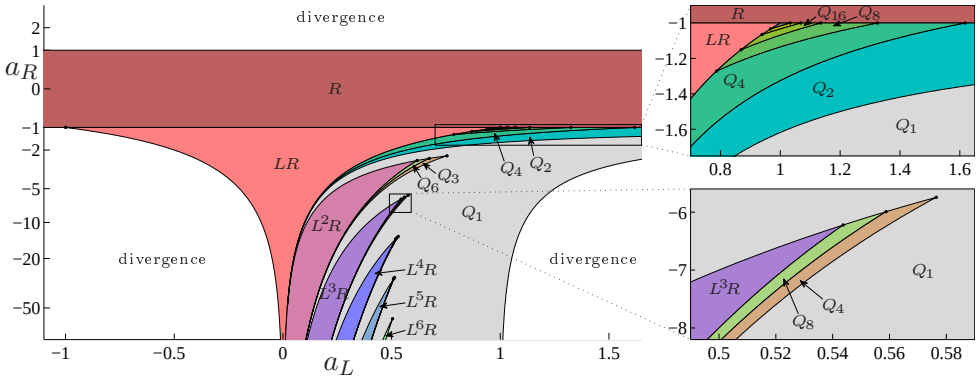

Figure 20: Attractors of the one-dimensional PWL map (11.1) for $\mu > 0$. In regions labelled $L^{n-1}R$, (11.1) has an attracting $L^{n-1}R$-cycle. In regions labelled Q_n, (11.1) has a chaotic attracting set comprised of n disjoint intervals.

In regions labelled Q_n there exists a chaotic set comprised of n disjoint intervals of $\mathbb{R}$. Formally the existence of a chaotic attractor for (1.4) can be proved by showing that there exists an attractor that is not a periodic solution [52]. The chaotic attractors exist in open regions of parameter space. That is, the chaos is *robust* [21].

In view of the symmetry property (3.12), attractors for $\mu < 0$ can be ascertained from Fig. 20 by switching the values of a_L and a_R. For example with $(a_L, a_R) = (-8, 0.25)$, (11.1) has an attracting R^2L-cycle for $\mu < 0$, because in Fig. 20 the point $(a_L, a_R) = (0.25, -8)$ lies in the L^2R-region.

For completeness we provide formulas for the bifurcation boundaries in Fig. 20. For derivations of these formulas the reader is referred to [132].

The LR-region is bounded by $a_R = -1$ and $a_R = \pm\frac{1}{a_L}$. For each $n \geq 3$, the $L^{n-1}R$-region is bounded on the left by a locus of BCBs, $a_R = -\frac{1-a_L^{n-1}}{a_L^{n-2}-a_L^{n-1}}$, and bounded on the right by $a_R = -\frac{1}{a_L^{n-1}}$, at which the stability multiplier of the $L^{n-1}R$-cycle is -1. Just beyond this bifurcation boundary, the curve $a_L^{2(n-1)}a_R^3 - a_R + a_L = 0$ bounds Q_{2n} and Q_n-regions, and the curve $a_L^{n-1}a_R^2 + a_R - a_L = 0$ bounds Q_n and Q_1-regions.

Next, let $\beta_0 = 1$, and for all $n \geq 0$, let $\beta_{n+1} = 2\beta_n + \frac{(-1)^n-1}{2}$. For all $n \geq 0$, Q_{2^n} and $Q_{2^{n+1}}$-regions are bounded by $a_L^{\beta_n}a_R^{\beta_{n+1}} + (-1)^n(a_R - a_L) = 0$. This sequence of curves limits to the point $(a_L, a_R) = (1, -1)$.

Finally, the boundary between Q_1 and the lower-right region labelled divergence (in which (11.1) has no attractor) is the curve $a_R = \frac{a_L}{1-a_L}$. On this boundary the critical point $x = 0$ maps to the fixed point $x^L = \frac{1}{1-a_L}$ in two iterations, and, as a consequence of kneading theory for one-dimensional maps [139], (11.1) has an unstable $\mathcal{S}$-cycle for every periodic symbol sequence $\mathcal{S}$.

11.2 The presence of a zero eigenvalue

As discussed in §2.1, dynamics near a grazing-sliding bifurcation is well-approximated by a map of the form (1.4) where one of the matrices A_L and A_R has a zero eigenvalue. Also, discrete-time economics models often involve PWL functions with flat segments [158], translating to a zero eigenvalue in either A_L or A_R.

If A_L has a zero eigenvalue of algebraic multiplicity 1, then the range of g^L is $(N-1)$-dimensional. For the purposes of studying the dynamics of (1.4) that involves both sides of the switching manifold, it suffices to study orbits of points on this $(N-1)$-dimensional surface. When $N = 2$, this provides substantial simplification, yet diverse dynamics is still possible. For instance, (1.4) can have mode-locking regions with shrinking points [183, 184], and chaotic attractors comprised of various numbers of disjoint pieces [113].

11.3 The volume-preserving case

Under a C^1 map, for instance g^L, the volume of an arbitrarily small set increases by a factor of $|\det(D_x g^L)|$. If $|\det(D_x g^L)| = 1$ everywhere, then g^L is *volume-preserving*. Consequently the PWL map (1.4) is volume-preserving if $\det(A_L) = \det(A_R) = 1$ or $\det(A_L) = \det(A_R) = -1$.

In each case (1.4) is invertible and so preserves the volume of sets intersecting the switching manifold.

If (1.4) is volume-preserving then it has no attractors and satisfies the Poincaré recurrence theorem [194]: for any $x_0 \in \mathbb{R}^N$, if the forward orbit $\{x_i\}$ is bounded, then for any neighbourhood of x_0, there exists $j \in \mathbb{Z}^+$ such that x_j is an element of this neighbourhood. Studies of (1.4) with $N = 2$ in the volume-preserving case have shown that there can exist regions of positive area within which the dynamics is ergodic [2, 47, 157, 196]. Dynamics with $N = 2$ in the volume-preserving case and $\mu = 0$ are analysed in detail in [117, 118, 119].

11.4 The effects of noise

By adding a small random component to an otherwise deterministic system, we can investigate how uncertainties and noise affect the dynamics. In general, small noise removes delicate dynamics, such as high-period solutions, but retains robust structures, including chaotic attractors. If the system has multiple attractors, with noise orbits may dwell close to one attractor then shift rapidly to the proximity of another attractor. Dwell times are roughly exponentially distributed with mean values that depend on the size of the basin of attraction, and on the strength of attraction [72, 111].

Here we consider the stochastic perturbation of (1.3)

$$x_{i+1} = \left\{ \begin{array}{ll} f^L(x_i;\mu,\eta)\,, & s_i \leq 0 \\ f^R(x_i;\mu,\eta)\,, & s_i \geq 0 \end{array} \right\} + \varepsilon\xi_i\,, \tag{11.2}$$

where the ξ_i are identically distributed, zero-mean, Gaussian random vectors, and $0 < \varepsilon \ll 1$ represents the noise amplitude. Suppose that in the absence of noise, the fixed point x^L is the global attractor of (11.2) and $s_L < 0$. Then for small $\varepsilon > 0$, the probability density function for the value of x_i for large i (given an initial point x_0 near x^L) is a roughly Gaussian invariant measure centred at x^L. This is because the bulk of the measure lies in the left half-space and so the switching manifold has little effect. Moreover, $\lim_{i\to\infty} \mathbb{E}[x_i] = x^L + O(\varepsilon^2)$ (where $\mathbb{E}$ denotes expectation) [78, 82]. However, if instead $s^L = 0$ then the difference between $\mathbb{E}[x_i]$ and x^L can be $O(\varepsilon)$ [96, 97]. In this case the noise effectively pushes orbits of (11.2) in a particular direction, on average.

Now suppose that in the absence of noise (11.2) has one attractor for $\mu < 0$ and two attractors for $\mu > 0$, and suppose that with $\varepsilon > 0$ we *dynamically* increase the value of μ slowly from an initially negative value, and look at the behaviour of an orbit. While $\mu < 0$, we can expect that the orbit is located near the unique attractor. However, as μ passes through zero, since all three attractors coincide with the origin at $\mu = 0$, we cannot say which attractor the orbit will be located near for $\mu > 0$ regardless of how small we set the value of ε. In this sense the behaviour of (11.2) is indeterminable as we pass through the BCB. If the rate at which we increase the value of μ is sufficiently slow, the orbit will most likely end up near the attractor that has a longer mean escape time [64].

For a particular application it may be more realistic to incorporate randomness in the switching condition, rather than additively as in (11.2). With this formulation the theory of iterated function systems can be used to prove the existence of an invariant measure [91].

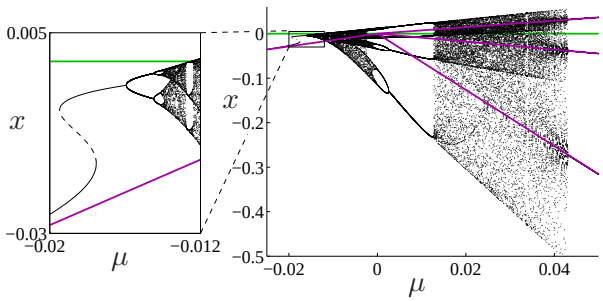

Figure 21: A bifurcation diagram of (11.3) with $\Phi(z) = \tanh(z)$, $f^L(x;\mu,\eta) = 0.3x + \mu$, $f^R(x;\mu,\eta) = -10x + \mu$ and $K = 100$. This map represents a smooth approximation to (11.1) with $(a_L, a_R) = (0.3, -10)$, which has an attracting fixed point for $\mu < 0$, and an attracting LLR-cycle for $\mu > 0$, as indicated with solid lines.

11.5 Smoothing

The map

$$x_{i+1} = \frac{1}{2}\left(f^L(x_i) + f^R(x_i)\right) - \frac{1}{2}\left(f^L(x_i) - f^R(x_i)\right)\Phi(Ks_i)\,, \tag{11.3}$$

represents a smooth approximation to (1.3), where $\Phi : \mathbb{R} \to \mathbb{R}$ is a smooth function with $\lim_{z\to\pm\infty}\Phi(z) = \pm 1$, and $K > 0$. The accuracy of the approximation is dictated by the magnitude of K. Since (11.3) is smooth, it exhibits familiar classical bifurcations. This suggests that by studying (11.3) as $K \to \infty$ we can interpret BCBs of (1.3) as the limit of one or more classical bifurcations. This is described for *discontinuous bifurcations* (the continuous-time analogue of BCBs) in [121, 122].

However, with large values of K the right hand-side of (11.3) has a steep derivative for $s_i \approx 0$, which causes difficulty for both analytical and numerical calculations. More importantly, smoothing can introduce new dynamics that is dependent on the choice of the function Φ, and so it is not clear that this approach can be useful for understanding BCBs.

For example, with $(a_L, a_R) = (0.3, -10)$ the one-dimensional map (11.1) has an attracting fixed point that changes to an attracting LLR-cycle at the BCB, Fig. 21. For $\mu < 0$, x^L is the only invariant set of (11.1). For $\mu > 0$, since (11.1) has a period-3 solution, it also has periodic solutions of every period [163], and chaotic dynamics [126]. The periodic solutions and chaos are all generated simultaneously at the BCB.

Fig. 21 also shows a bifurcation diagram of the corresponding smoothed map (11.3) using $\Phi(z) = \tanh(z)$. For this map the transition from period-1 to period-3 requires an infinite sequence of bifurcations. The map (11.3) has an attracting period-3 solution for all values of μ greater than about 0.043. In addition, as shown in the inset of Fig. 21, the smoothing has generated additional fixed points, as described in [102]. The smoothing of PWS maps has also been found to eliminate robust chaos by generating windows of periodicity [46].

12 Summary and outlook

The theory of BCBs provides an important building block for the growing field of nonsmooth dynamical systems in which simple and complex dynamical behaviour is generated in fundamentally different manners to that of smooth dynamical systems. For instance, at a BCB a stable fixed point can instantly transition to a chaotic attractor. This was observed in DC/DC converters [76] before subsequently being explained through an understanding of BCBs [54, 198]. Alternatively, at a BCB a stable fixed point can split into several attractors. All attractors created in BCBs grow asymptotically linearly in size with respect to parameter change.

Structurally stable invariant sets created in a BCB are captured by a PWL map of the form (1.4). The nature of the dynamics on both sides of the BCB is determined by the eigenvalues of the matrices A_L and A_R in (1.4). More precisely, given two maps (1.4) that share the same two sets of eigenvalues, if both maps are observable and $\varrho^{\mathsf{T}} b \neq 0$, see §5.4, then the maps are affinely conjugate (that is, there exists an affine coordinate change that transforms one map to the other and does not alter the switching manifold).

The simplest invariant sets of (1.4) are fixed points and period-two solutions. There are four non-degenerate scenarios for the existence and relative coexistence of these solutions, as determined by two simple conditions on the eigenvalues of A_L and A_R. This is summarised by Table 1. An analogous classification of other dynamical features for general N appears to be impractical. Complicated dynamics can occur on one or both sides of a BCB.

Several different mechanisms for the creation of exotic dynamics at BCBs have been reviewed in this paper. In a neighbourhood of a BCB there may be a unique fixed point that is stable for all parameter values except at the BCB. This is termed a dangerous bifurcation and is due to the presence of an attractor at infinity for the PWL approximation to the BCB, §7.5. Mode-locking regions of attracting solutions generated in BCBs commonly exhibit a distinctive chain structure. This is due to boundaries of mode-locking regions intersecting at points where a periodic solution has two points on the switching manifold, and applies to periodic solutions that, at least in a symbolic sense, correspond to rigid rotation on a circle, §9.3. Infinitely many attractors can be created simultaneously at codimension-three BCBs for which a periodic orbit has a coincident homoclinic connection, §7.2, and multi-dimensional attractors are also possible, §7.3.

Many interesting problems remain for future work. Here is a short list of some such problems.

i) A qualitative description of the chain structure of mode-locking regions can be inferred from Theorem 9.2, but a quantitative description of the global layout of the mode-locking regions is not known. It would be helpful to understand, for instance, scaling laws that govern the distribution of shrinking points throughout a generic two-parameter cross-section of parameter space.

ii) Attracting $\mathcal{S}$-cycles can be created in BCBs in $\mathbb{R}^N$ for only certain periodic symbol sequences $\mathcal{S}$. With $N = 1$ an attracting $\mathcal{S}$-cycle can be found for some combination of parameter values if and only if $\mathcal{S}$ either has at most one L or at most one R, §11.1. It remains to characterise such periodic symbol sequences for $N \geq 2$.

iii) For smooth dynamical systems, homoclinic connections are created at homoclinic tangencies and are a fundamental mechanism by which chaotic dynamics is generated. Near BCBs, homoclinic connections are typically created at homoclinic corners, §10.2. These may be

thought of as continuous but non-differentiable distortions of homoclinic tangencies, so have many similarities to homoclinic tangencies, but have not yet been investigated rigorously.

iv) Theorem 8.3 describes the basic bifurcations associated with the codimension-two coincidence of a BCB and a Neimark-Sacker bifurcation in $\mathbb{R}^N$. However, even with $N = 2$, which is the smallest value of N possible for this scenario, a complete classification of the associated dynamics is not known. In particular, dynamics relating to the collision of an invariant circle of (1.3) with a switching manifold, which occurs near this scenario, does not appear to have been explored.

v) Dimension reduction via a classical centre manifold analysis is not possible for BCBs. However, if (1.3) has parameters with varying orders of magnitude, an approximate dimension reduction might be possible in a manner akin to geometric singular perturbation theory.

We have seen that dynamical behaviour associated with BCBs can be extremely complicated. For instance, an N-dimensional invariant set can be created in a BCB in $\mathbb{R}^N$, §7.3. Yet the equations that govern the dynamics are merely PWL, and so various calculations that need to be performed numerically for analogous smooth maps, can here be achieved exactly, albeit often using computer algebra. For this reason, some aspects of nonlinear dynamics can be explored analytically when the dynamics is created in a BCB rather than in a classical bifurcation of a smooth map. A solid framework for understanding BCBs has been established, but as described above various features remain to be explained. One can also explore generalisations, such as BCBs for maps on tori, and PWL continuous maps comprised of more than two pieces [33, 84, 133].

References

[1] V.S. Afraimovich and L.P. Shil'nikov. Invariant two-dimensional tori, their breakdown and stochasticity. *Amer. Math. Soc. Transl.*, 149:201–212, 1991. translation of article published in *Methods of Qualitative Theory of Differential Equations*. Gorki University Press, Gorki, 1983.

[2] D. Aharonov, R.L. Devaney, and U. Elias. The dynamics of a piecewise linear map and its smooth approximation. *Int. J. Bifurcation Chaos*, 7(2):351–372, 1997.

[3] P. Alessandri and V. Berthé. Three distance theorems and combinatorics on words. *Enseign. Math.*, 44:103–132, 1998.

[4] J.A. Amador, G. Olivar, and F. Angulo. Smooth and Filippov models of sustainable development: Bifurcations and numerical computations. *Differ. Equ. Dyn. Syst.*, 21:173–184, 2013.

[5] F. Angulo, M. di Bernardo, S.J. Hogan, P. Kowalczyk, and G. Olivar. Two-parameter non-smooth bifurcations in power converters. *IEEE Int. Symp. Circ. Syst.*, pages 1485–1488, 2005. Kobe, Japan, 23-26 May.

[6] F. Angulo, G. Olivar, and M. di Bernardo. Two-parameter discontinuity-induced bifurcation curves in a ZAD-strategy-controlled DC-DC buck converter. *IEEE Trans. Circuits Systems I Fund. Theory Appl.*, 55(8):2392–2401, 2008.

[7] V.I. Arnol'd. Small denominators. I. Mappings of the circumference onto itself. *Amer. Math. Soc. Transl. Ser. 2*, 46:213–284, 1965. Translation of *Izvest. Akad. Nauk SSSR Ser. Mat.*, 25:1-86, 1961.

[8] V.I. Arnol'd. *Geometrical Methods in the Theory of Ordinary Differential Equations*. Springer-Verlag, New York, 1988.

[9] D.G. Aronson, M.A. Chory, G.R. Hall, and R.P. McGehee. Bifurcations from an invariant circle for two-parameter families of maps of the plane: A computer-assisted study. *Comm. Math. Phys.*, 83:303–354, 1982.

[10] V. Avrutin, P.S. Dutta, M. Schanz, and S. Banerjee. Influence of a square-root singularity on the behaviour of piecewise smooth maps. *Nonlinearity*, 23:445–463, 2010.

[11] V. Avrutin and M. Schanz. Period-doubling scenario without flip bifurcations in a one-dimensional map. *Int. J. Bifurcation Chaos*, 15(4):1267–1284, 2005.

[12] V. Avrutin and M. Schanz. On the fully developed bandcount adding scenario. *Nonlinearity*, 21:1077–1103, 2008.

[13] V. Avrutin, M. Schanz, and S. Banerjee. Codimension-three bifurcations: Explanation of the complex one-, two-, and three-dimensional bifurcation structures in nonsmooth maps. *Phys. Rev. E.*, 75:066205, 2007.

[14] V. Avrutin, M. Schanz, and L. Gardini. Calculation of bifurcation curves by map replacement. submitted: Int. J. Bifurcation Chaos.

[15] V. Avrutin, M. Schanz, and L. Gardini. On a special type of border-collision bifurcations occurring at infinity. *Phys. D*, 239:1083–1094, 2010.

[16] J. Awrejcewicz and C. Lamarque. *Bifurcation and Chaos in Nonsmooth Mechanical Systems.* World Scientific, Singapore, 2003.

[17] S. Banerjee and C. Grebogi. Border collision bifurcations in two-dimensional piecewise smooth maps. *Phys. Rev. E*, 59(4):4052–4061, 1999.

[18] S. Banerjee, M.S. Karthik, G. Yuan, and J.A. Yorke. Bifurcations in one-dimensional piecewise smooth maps - Theory and applications in switching circuits. *IEEE Trans. Circuits Systems I Fund. Theory Appl.*, 47(3):389–394, 2000.

[19] S. Banerjee, P. Ranjan, and C. Grebogi. Bifurcations in two-dimensional piecewise smooth maps - Theory and applications in switching circuits. *IEEE Trans. Circuits Systems I Fund. Theory Appl.*, 47(5):633–643, 2000.

[20] S. Banerjee and G.C. Verghese, editors. *Nonlinear Phenomena in Power Electronics.* IEEE Press, New York, 2001.

[21] S. Banerjee, J.A. Yorke, and C. Grebogi. Robust chaos. *Phys. Rev. Lett.*, 80(14):3049–3052, 1998.

[22] S. Barnett. *Introduction to Mathematical Control Theory.* Clarendon Press, Oxford, 1975.

[23] S.K. Berberian. *Linear Algebra.* Oxford University Press, New York, 1992.

[24] B. Blazejczyk-Okolewska, K. Czolczynski, T. Kapitaniak, and J. Wojewoda. *Chaotic Mechanics in Systems with Impacts and Friction.* World Scientific, Singapore, 1999.

[25] H. Broer and M. Levi. Geometrical aspects of stability theory for Hill's equations. *Arch. Rational Mech. Anal.*, 131:225–240, 1995.

[26] B. Brogliato. *Nonsmooth Mechanics: Models, Dynamics and Control.* Springer-Verlag, New York, 1999.

[27] V.A. Brousin, Yu.I. Neimark, and M.I. Feigin. On some cases of dependence of periodic motions of relay system upon parameters. *Izv. Vyssh. Uch. Zav. Radiofizika*, 4:785–800, 1963. In Russian.

[28] J. Caballé, X. Jarque, and E. Michetti. Chaotic dynamics in credit constrained emerging economies. *J. Econ. Dyn. Control*, 30:1261–1275, 2006.

[29] J.L. Cabrera and J.G. Milton. On-off intermittency in a human balancing task. *Phys. Rev. Lett.*, 89(15):158702, 2002.

[30] D.K. Campbell, R. Galeeva, C. Tresser, and D.J. Uherka. Piecewise linear models for the quasiperiodic transition to chaos. *Chaos*, 6(2):121–154, 1996.

[31] V. Carmona, E. Freire, E. Ponce, and F. Torres. On simplifying and classifying piecewise-linear systems. *IEEE Trans. Circuits Systems I Fund. Theory Appl.*, 49(5):609–620, 2002.

[32] V. Carmona, E. Freire, E. Ponce, and F. Torres. The continuous matching of two stable linear systems can be unstable. *Disc. Cont. Dyn. Sys.*, 16(3):689–703, 2006.

[33] H. Chang and J. Juang. Piecewise two-dimensional maps and applications to cellular neural networks. *Int. J. Bifurcation Chaos*, 14(7):2223–2228, 2004.

[34] W. Chin, E. Ott, H.E. Nusse, and C. Grebogi. Grazing bifurcations in impact oscillators. *Phys. Rev. E*, 50(6):4427–4450, 1994.

[35] A. Colombo. Boundary intersection crossing bifurcation in the presence of sliding. *Phys. D*, 237:2900–2912, 2008.

[36] A. Colombo and F. Dercole. Discontinuity induced bifurcations of non-hyperbolic cycles in nonsmooth systems. *SIAM J. Appl. Dyn. Sys.*, 9(1):62–83, 2010.

[37] A. Colombo, M. di Bernardo, S.J. Hogan, and M.R. Jeffrey. Bifurcations of piecewise smooth flows: Perspectives, methodologies and open problems. *Phys. D*, 241(22):1845–1860, 2012.

[38] A. Colombo, M. di Bernardo, S.J. Hogan, and P. Kowalczyk. Complex dynamics in a hysteretic relay feedback system with delay. *J. Nonlinear Sci.*, 17:85–108, 2007.

[39] S. Coombes and A.H. Osbaldestin. Period-adding bifurcations and chaos in a periodically stimulated excitable neural relaxation oscillator. *Phys. Rev. E*, 62(3):4057–4066, 2000.

[40] M. Courtemanche, L. Glass, J. Bélair, D. Scagliotti, and D. Gordon. A circle map in a human heart. *Phys. D*, 40:299–310, 1989.

[41] F.B. Cunha, D.J. Pagano, and U.F. Moreno. Sliding bifurcations of equilibria in planar variable structure systems. *IEEE Trans. Circuits Systems I Fund. Theory Appl.*, 50(8):1129–1134, 2003.

[42] S. De, P.S. Dutta, S. Banerjee, and A.R. Roy. Local and global bifurcations in three-dimensional, continuous, piecewise-smooth maps. *Int. J. Bifurcation Chaos*, 21(6):1617–1636, 2011.

[43] O. Decroly and A. Goldbeter. From simple to complex oscillatory behaviour: Analysis of bursting in a multiply regulated biochemical system. *J. Theor. Biol.*, 124:219–250, 1987.

[44] F. Dercole, A. Gragnani, Yu.A. Kuznetsov, and S. Rinaldi. Numerical sliding bifurcation analysis: An application to a relay control system. *IEEE Trans. Circuits Systems I Fund. Theory Appl.*, 50(8):1058–1063, 2003.

[45] F. Dercole, A. Gragnani, and S. Rinaldi. Bifurcation analysis of piecewise smooth ecological models. *Theor. Popul. Biol.*, 72:197–213, 2007.

[46] A. Deshpande, Q. Chen, Y. Wang, Y.-C. Lai, and Y. Do. Effect of smoothing on robust chaos. *Phys. Rev. E*, 82:026209, 2010.

[47] R.L. Devaney. A piecewise linear model for the zones of instability of an area-preserving map. *Phys. D*, 10(3):387–393, 1984.

[48] M. di Bernardo. Normal forms of border collision in high dimensional non-smooth maps. In *Proceedings IEEE ISCAS, Bangkok, Thailand*, volume 3, pages 76–79, 2003.

[49] M. di Bernardo, C.J. Budd, and A.R. Champneys. Grazing, skipping and sliding: Analysis of the non-smooth dynamics of the DC/DC buck converter. *Nonlinearity*, 11:859–890, 1998.

[50] M. di Bernardo, C.J. Budd, and A.R. Champneys. Corner collision implies border-collision bifurcation. *Phys. D*, 154:171–194, 2001.

[51] M. di Bernardo, C.J. Budd, and A.R. Champneys. Normal form maps for grazing bifurcations in n-dimensional piecewise-smooth dynamical systems. *Phys. D*, 160:222–254, 2001.

[52] M. di Bernardo, C.J. Budd, A.R. Champneys, and P. Kowalczyk. *Piecewise-smooth Dynamical Systems. Theory and Applications.* Springer-Verlag, New York, 2008.

[53] M. di Bernardo, M.I. Feigin, S.J. Hogan, and M.E. Homer. Local analysis of C-bifurcations in n-dimensional piecewise-smooth dynamical systems. *Chaos Solitons Fractals*, 10(11):1881–1908, 1999.

[54] M. di Bernardo, F. Garofalo, L. Glielmo, and F. Vasca. Switchings, bifurcations and chaos in DC/DC converters. *IEEE Trans. Circuits Systems I Fund. Theory Appl.*, 45(2):133–141, 1998.

[55] M. di Bernardo, F. Garofalo, L. Iannelli, and F. Vasca. Bifurcations in piecewise-smooth feedback systems. *Internat. J. Control*, 75(16-17):1243–1259, 2002.

[56] M. di Bernardo, K.H. Johansson, U. Jönsson, and F. Vasca. On the robustness of periodic solutions in relay feedback systems. In *15th Triennial World Congress, Barcelona, Spain*, 2002.

[57] M. di Bernardo, K.H. Johansson, and F. Vasca. Self-oscillations and sliding in relay feedback systems: Symmetry and bifurcations. *Int J. Bifurcation Chaos*, 11(4):1121–1140, 2001.

[58] M. di Bernardo, P. Kowalczyk, and A. Nordmark. Bifurcations of dynamical systems with sliding: Derivation of normal-form mappings. *Phys. D*, 170:175–205, 2002.

[59] M. di Bernardo, P. Kowalczyk, and A. Nordmark. Sliding bifurcations: A novel mechanism for the sudden onset of chaos in dry friction oscillators. *Int. J. Bifurcation Chaos*, 13(10):2935–2948, 2003.

[60] M. di Bernardo, U. Montanaro, and S. Santini. Canonical forms of generic piecewise linear continuous systems. *IEEE Trans. Automat. Contr.*, 56(8):1911–1915, 2011.

[61] Y. Do. A mechanism for dangerous border collision bifurcations. *Chaos Solitons Fractals*, 32:352–362, 2007.

[62] Y. Do and H.K. Baek. Dangerous border-collision bifurcations of a piecewise-smooth map. *Comm. Pure Appl. Anal.*, 5(3):493–503, 2006.

[63] Y. Do, S.D. Kim, and P.S. Kim. Stability of fixed points placed on the border in the piecewise linear systems. *Chaos Solitons Fractals*, 38(2):391–399, 2008.

[64] M. Dutta, H.E. Nusse, E. Ott, J.A. Yorke, and G. Yuan. Multiple attractor bifurcations: A source of unpredictability in piecewise smooth systems. *Phys. Rev. Lett.*, 83(21):4281–4284, 1999.

[65] P.S. Dutta, S. De, S. Banerjee, and A.R. Roy. Torus destruction via global bifurcations in a piecewise-smooth, continuous map with square-root nonlinearity. *Phys. Lett. A*, 373:4426–4433, 2009.

[66] P.S. Dutta, B. Routroy, S. Banerjee, and S.S. Alam. On the existence of low-period orbits in n-dimensional piecewise linear discontinuous maps. *Nonlinear Dynamics*, 53:369–380, 2008.

[67] F.W. Fairman. *Linear Control Theory. The State Space Approach.* Wiley, New York, 1998.

[68] O. Feely, D. Fournier-Prunaret, I. Taralova-Roux, and D. Fitzgerald. Nonlinear dynamics of bandpass sigma-delta modulation. an investigation by means of the critical lines tool. *Int. J. Bifurcation Chaos*, 10:307–323, 2000.

[69] M.I. Feigin. Doubling of the oscillation period with C-bifurcations in piecewise continuous systems. *J. Appl. Math. Mech.*, 34(5):822–830, 1970. Translation of *Prikl. Mat. Mekh.*, 34(5):861-869, 1970.

[70] M.I. Feigin. On the structure of C-bifurcation boundaries of piecewise-continuous systems. *J. Appl. Math. Mech.*, 42(5):885–895, 1978. Translation of *Prikl. Mat. Mekh.*, 42(5):820-829, 1978.

[71] N. Fenichel. Persistence and smoothness of invariant manifolds for flows. *Indiana Univ. Math. J.*, 21(3), 1971.

[72] U. Feudel. Complex dynamics in multistable systems. *Int. J. Bifurcation Chaos*, 18(6):1607–1626, 2008.

[73] A.F. Filippov. Differential equations with discontinuous right-hand side. *Mat. Sb.*, 51(93):99–128, 1960. English transl. *Amer. Math. Soc. Transl.* 42(2):199–231, 1964.

[74] A.F. Filippov. *Differential Equations with Discontinuous Righthand Sides.* Kluwer Academic Publishers., Norwell, 1988.

[75] N.P. Fogg. *Substitutions in Dynamics, Arithmetics and Combinatorics.* Springer-Verlag, New York, 2002.

[76] E. Fossas and G. Olivar. Study of chaos in the buck converter. *IEEE Trans. Circuits Systems I Fund. Theory Appl.*, 43(1):13–25, 1996.

[77] M.H. Fredriksson and A.B. Nordmark. On normal form calculation in impact oscillators. *Proc. R. Soc. A*, 456:315–329, 2000.

[78] M.I. Freidlin and A.D. Wentzell. *Random Perturbations of Dynamical Systems.* Springer, New York, 2012.

[79] C.E. Frouzakis, L. Gardini, I.G. Kevrekidis, G. Millerioux, and Mira C. On some properties of invariant sets of two-dimensional noninvertible maps. *Int. J. Bifurcation Chaos*, 7(6):1167–1194, 1997.

[80] M. Gallegati, L. Gardini, T. Puu, and I. Sushko. Hicks' trade cycle revisited: Cycles and bifurcations. *Math. Comput. Simulation*, 63:505–527, 2003.

[81] A. Ganguli and S. Banerjee. Dangerous bifurcation at border collision: When does it occur? *Phys. Rev. E.*, 71(5):057202, 2005.

[82] C.W. Gardiner. *Stochastic Methods. A Handbook for the Natural and Social Sciences.* Springer, New York, 2009.

[83] L. Gardini. Some global bifurcations of two-dimensional endomorphisms by use of critical lines. *Nonlinear Anal.*, 18(4):361–399, 1992.

[84] L. Gardini, T. Puu, and I. Sushko. The Hicksian model with investment floor and income ceiling. In [158], pages 179-191.

[85] L. Gardini, F. Tramontana, V. Avrutin, and M. Schanz. Border collision bifurcations in 1D piecewise-linear maps and Leonov's approach. submitted: Int. J. Bifurcation Chaos.

[86] P. Gaspard and X.-J. Wang. Homoclinic orbits and mixed-mode oscillations in far-from-equilibrium systems. *J. Stat. Phys.*, 48:151–199, 1987.

[87] N.K. Gavrilov and L.P. Šil'nikov. On three-dimensional dynamical systems close to systems with a structurally unstable homoclinic curve I. *Mat. USSR Sb.*, 17:467–485, 1972.

[88] N.K. Gavrilov and L.P. Šil'nikov. On three-dimensional dynamical systems close to systems with a structurally unstable homoclinic curve II. *Mat. USSR Sb.*, 19:139–156, 1973.

[89] L. Glass and M.C. Mackey. A simple model for phase locking of biological oscillators. *J. Math. Biology*, 7:339–352, 1979.

[90] P. Glendinning. Bifurcations of snap-back repellers with application to border-collision bifurcations. *Int. J. Bifurcation Chaos*, 20:479–489, 2010.

[91] P. Glendinning. The border collision normal form with stochastic switching surface. *SIAM J. Appl. Dyn. Sys.*, 13(1):181–193, 2014.

[92] P. Glendinning and M.R. Jeffrey. Grazing-sliding bifurcations, border collision maps and the curse of dimensionality for piecewise smooth bifurcation theory. *Nonlinearity*, 28:263–283, 2015.

[93] P. Glendinning, P. Kowalczyk, and A.B. Nordmark. Attractors near grazing-sliding bifurcations. *Nonlinearity*, 25:1867–1885, 2012.

[94] P. Glendinning and C.H. Wong. Border collision bifurcations, snap-back repellers, and chaos. *Phys. Rev. E*, 79:025202, 2009.

[95] P. Glendinning and C.H. Wong. Two dimensional attractors in the border collision normal form. *Nonlinearity*, 24:995–1010, 2011.

[96] T. Griffin and S. Hogan. Dynamics of discontinuous systems with imperfections and noise. In G. Rega and F. Vestroni, editors, *IUTAM Symposium on Chaotic Dynamics and Control of Systems and Processes in Mechanics.*, pages 275–285. Springer, 2005.

[97] T.C.L. Griffin and S.J. Hogan. The effects of noise on a piecewise linear map. In preparation., 2012.

[98] M. Guardia, S.J. Hogan, and T.M. Seara. An analytical approach to codimension-2 sliding bifurcations in the dry friction oscillator. *Unpublished*, 2009.

[99] C. Halse, M. Homer, and M. di Bernardo. C-bifurcations and period-adding in one-dimensional piecewise-smooth maps. *Chaos Solitons Fractals*, 18:953–976, 2003.

[100] M.A. Hassouneh, E.H. Abed, and H.E. Nusse. Robust dangerous border-collision bifurcations in piecewise smooth systems. *Phys. Rev. Lett.*, 92:070201, 2004.

[101] M.W. Hirsch, C.C. Pugh, and M. Shub. *Invariant Manifolds.*, volume 583 of *Lecture Notes in Mathematics.* Springer-Verlag, New York, 1977.

[102] S.J. Hogan. The effect of smoothing on bifurcation and chaos computations in non-smooth mechanics. In *Proceedings of the XXI International Congress of Theoretical and Applied Mathematics.*, 2004.

[103] S.J. Hogan, L. Higham, and T.C.L. Griffin. Dynamics of a piecewise linear map with a gap. *Proc. R. Soc. A*, 463:49–65, 2007.

[104] C.H. Hommes and H.E. Nusse. "Period three to period two" bifurcation for piecewise linear models. *J. Economics*, 54(2):157–169, 1991.

[105] C.H. Hommes, H.E. Nusse, and A. Simonovits. Cycles and chaos in a socialist economy. *J. Econ. Dyn. Control*, 19:155–179, 1995.

[106] P. Jain and S. Banerjee. Border-collision bifurcations in one-dimensional discontinuous maps. *Int. J. Bifurcation Chaos*, 13(11):3341–3351, 2003.

[107] M.R. Jeffrey and S.J. Hogan. The geometry of generic sliding bifurcations. *SIAM Rev.*, 53(3):505–525, 2011.

[108] M. Johansson. *Piecewise Linear Control Systems.*, volume 284 of *Lecture Notes in Control and Information Sciences.* Springer-Verlag, New York, 2003.

[109] T. Kapitaniak and Yu. Maistrenko. Multiple choice bifurcations as a source of unpredictability in dynamical systems. *Phys. Rev. E*, 58(4):5161–5163, 1998.

[110] J. Keener. Chaotic behavior in piecewise continuous difference equations. *Trans. Amer. Math. Soc.*, 261(2):589–604, 1980.

[111] E. Knobloch and J.B. Weiss. Effect of noise on discrete dynamical systems with multiple attractors. In M.F. McClintock and P.V.E. Moss, editors, *Noise in Nonlinear Dynamical Systems. Theory of noise induced processes in special applications.*, volume 2, pages 65–86. Cambridge University Press, New York, 1989.

[112] B. Kolman. *Elementary Linear Algebra.* Prentice Hall, Upper Saddle River, NJ, 1996.

[113] P. Kowalczyk. Robust chaos and border-collision bifurcations in non-invertible piecewise-linear maps. *Nonlinearity*, 18:485–504, 2005.

[114] P. Kowalczyk and P.T. Piiroinen. Two-parameter sliding bifurcations of periodic solutions in a dry-friction oscillator. *Phys. D*, 237:1053–1073, 2008.

[115] Yu.A. Kuznetsov. *Elements of Bifurcation Theory.*, volume 112 of *Appl. Math. Sci.* Springer-Verlag, New York, 2004.

[116] Yu.A. Kuznetsov, S. Rinaldi, and A. Gragnani. One-parameter bifurcations in planar Filippov systems. *Int. J. Bifurcation Chaos*, 13(8):2157–2188, 2003.

[117] J.C. Lagarias and E. Rains. Dynamics of a family of piecewise-linear area-preserving plane maps. I. Rational rotation numbers. *J. Difference Eqn. Appl.*, 11(12):1089–1108, 2005.

[118] J.C. Lagarias and E. Rains. Dynamics of a family of piecewise-linear area-preserving plane maps. II. Invariant circles. *J. Difference Eqn. Appl.*, 11(13):1137–1163, 2005.

[119] J.C. Lagarias and E. Rains. Dynamics of a family of piecewise-linear area-preserving plane maps. III. Cantor set spectra. *J. Difference Eqn. Appl.*, 11(14):1205–1224, 2005.

[120] J. Laugesen and E. Mosekilde. Border-collision bifurcations in a dynamic management game. *Comput. Oper. Res.*, 33:464–478, 2006.

[121] R.I. Leine. Bifurcations of equilibria in non-smooth continuous systems. *Phys. D*, 223:121–137, 2006.

[122] R.I. Leine and H. Nijmeijer. *Dynamics and Bifurcations of Non-smooth Mechanical Systems*, volume 18 of *Lecture Notes in Applied and Computational Mathematics*. Springer-Verlag, Berlin, 2004.

[123] R.I. Leine and D.H. Van Campen. Discontinuous bifurcations of periodic solutions. *Math. Comput. Model.*, 36:259–273, 2002.

[124] R.I. Leine, D.H. Van Campen, and B.L. Van de Vrande. Bifurcations in nonlinear discontinuous systems. *Nonlinear Dynamics*, 23:105–164, 2000.

[125] N.N. Leonov. Discontinuous map of the straight line. *Dokl. Akad. Nauk. SSSR*, 143:1038–1041, 1962. In Russian.

[126] T. Li and J.A. Yorke. Period three implies chaos. *Amer. Math. Monthly.*, 82(10):985–992, 1975.

[127] R. Lozi. Un attracteur étrange(?) du type attracteur de Hénon. *J. Phys. (Paris)*, 39(C5):9–10, 1978. In French.

[128] M. Lyubich. Combinatorics, geometry and attractors of quasi-quadratic maps. *Ann. Math.*, 140(2):347–404, 1994.

[129] Y. Ma, M. Agarwal, and S. Banerjee. Border collision bifurcations in a soft impact system. *Phys. Lett. A*, 354:281–287, 2006.

[130] Y. Ma, J. Ing, S. Banerjee, M. Wiercigroch, and E. Pavlovskaia. The nature of the normal form map for soft impacting systems. *Int. J. Nonlinear Mech.*, 43:504–513, 2008.

[131] Y. Maistrenko, I. Sushko, and L. Gardini. About two mechanisms of reunion of chaotic attractors. *Chaos Solitons Fractals*, 9(8):1373–1390, 1998.

[132] Yu.L. Maistrenko, V.L. Maistrenko, and L.O. Chua. Cycles of chaotic intervals in a time-delayed Chua's circuit. *Int. J. Bifurcation Chaos.*, 3(6):1557–1572, 1993.

[133] Yu.L. Maistrenko, V.L. Maistrenko, S.I. Vikul, and L.O. Chua. Bifurcations of attracting cycles from time-delayed Chua's circiut. *Int. J. Bifurcation Chaos.*, 5(3):653–671, 1995.

[134] F.R. Marotto. Snap-back repellers imply chaos in $\mathbb{R}^n$. *J. Math. Anal. Appl.*, 63:199–223, 1978.

[135] F.R. Marotto. On redefining a snap-back repeller. *Chaos Solitons Fractals*, 25:25–28, 2005.

[136] M. McGuinness, Y. Hong, D. Galletly, and P. Larsen. Arnold tongues in human cardiorespiratory systems. *Chaos*, 14(1):1–6, 2004.

[137] J.D. Meiss. *Differential Dynamical Systems.* SIAM, Philadelphia, 2007.

[138] R. Mettin, U. Parlitz, and W. Lauterborn. Bifurcation structure of the driven van der Pol oscillator. *Int. J. Bifurcation Chaos*, 3(6):1529–1555, 1993.

[139] J. Milnor and W. Thurston. On iterated maps of the interval. In A. Dold and B. Eckmann, editors, *Lect. Notes. in Math.*, volume 1342, pages 465–563, New York, 1988. Springer-Verlag.

[140] C. Mira, L. Gardini, A. Barugola, and J. Cathala. *Chaotic Dynamics in Two-Dimensional Noninvertible Maps.*, volume 20 of *Nonlinear Science*. World Scientific, Singapore, 1996.

[141] C. Mira, C. Rauzy, Y. Maistrenko, and I. Sushko. Some properties of a two-dimensional piecewise-linear noninvertible map. *Int. J. Bifurcation Chaos*, 6(12a):2299–2320, 1996.

[142] M. Misiurewicz. Strange attractors for the Lozi mappings. In R.G. Helleman, editor, *Nonlinear dynamics, Annals of the New York Academy of Sciences*, pages 348–358, 1980.

[143] J. Molenaar, J.G. de Weger, and W. van de Water. Mappings of grazing-impact oscillators. *Nonlinearity*, 14:301–321, 2001.

[144] M. Morse and G.A. Hedlund. Symbolic dynamics II. Sturmian trajectories. *Am. J. Math.*, 62:1–42, 1940.

[145] A.B. Nordmark. Non-periodic motion caused by grazing incidence in impact oscillators. *J. Sound Vib.*, 2:279–297, 1991.

[146] A.B. Nordmark. Universal limit mapping in grazing bifurcations. *Phys. Rev. E*, 55(1):266–270, 1997.

[147] A.B. Nordmark. Existence of periodic orbits in grazing bifurcations of impacting mechanical oscillators. *Nonlinearity*, 14:1517–1542, 2001.

[148] H.E. Nusse and J.A. Yorke. Border-collision bifurcations including "period two to period three" for piecewise smooth systems. *Phys. D*, 57:39–57, 1992.

[149] H.E. Nusse and J.A. Yorke. Border-collision bifurcations for piecewise-smooth one-dimensional maps. *Int. J. Bifurcation Chaos.*, 5(1):189–207, 1995.

[150] G. Osorio, M. di Bernardo, and S. Santini. Corner-impact bifurcations: A novel class of discontinuity-induced bifurcations in cam-follower systems. *SIAM J. Appl. Dyn. Sys.*, 7(1):18–38, 2008.

[151] G. Ostrovski. Dynamics of a continuous piecewise affine map of the square. *Unpublished*, 2013.

[152] J. Palis and F. Takens. *Hyperbolicity and sensitive chaotic dynamics at homoclinic bifurcations.* Cambridge University Press, New York, 1993.

[153] W. Perruquetti and J.P. Barbot, editors. *Sliding Mode Control in Engineering.* Marcel Dekker, New York, 2002.

[154] S.H. Piltz, M.A. Porter, and P.K. Maini. Prey switching with a linear preference trade-off. *SIAM J. Appl. Dyn. Sys.*, 13(2):658–682, 2014.

[155] A.S. Poznyak. *Advanced Mathematical Tools for Automatic Control Engineers. Deterministic Techniques.* Elsevier, Amsterdam, 2008.

[156] T. Puu, L. Gardini, and I. Sushko. A Hicksian multiplier-accelerator model with floor determined by capital stock. *J. Econ. Behav. Organ.*, 56:331–348, 2005.

[157] T. Puu, L. Gardini, and I. Sushko. On the change of periodicities in the Hicksian multiplier-accelerator model with a consumption floor. *Chaos Solitons Fractals*, 29:681–696, 2006.

[158] T. Puu and I. Sushko, editors. *Business Cycle Dynamics: Models and Tools.* Springer-Verlag, New York, 2006.

[159] B. Rakshit, M. Apratim, and S. Banerjee. Bifurcation phenomena in two-dimensional piecewise smooth discontinuous maps. *Chaos*, 20:033101, 2010.

[160] C. Robinson. *Dynamical Systems. Stability, Symbolic Dynamics, and Chaos.* CRC Press, Boca Raton, FL, 1999.

[161] Y.-H. Roh and J.-H. Oh. Robust stabilization of uncertain input-delay systems by sliding mode control with delay compensation. *Automatica*, 35:1861–1865, 1999.

[162] N.F. Rulkov. Modeling of spiking-bursting neural behavior using two-dimensional map. *Phys. Rev. E*, 65:041922, 2002.

[163] A.N. Sharkovskii. Co-existence of cycles of a continuous map of the line to itself. *Int. J. Bifurcation Chaos*, 5(5):1263–1273, 1995. Translation of *Ukrain. Mat. Z.*, 16:61-71, 1964.

[164] Y. Shi and P. Yu. Chaos induced by regular snap-back repellers. *J. Math. Anal. Appl.*, 337:1480–1494, 2008.

[165] J. Sieber. Dynamics of delayed relay systems. *Nonlinearity*, 19(11):2489–2527, 2006.

[166] J. Sieber, P. Kowalczyk, S.J. Hogan, and M. di Bernardo. Dynamics of symmetric dynamical systems with delayed switching. *J. Vib. Control*, 16(7-8):1111–1140, 2010.

[167] R.M. Siegel, C. Tresser, and G. Zettler. A decoding problem in dynamics and in number theory. *Chaos*, 2(4):473–493, 1992.

[168] D.J.W. Simpson. *Bifurcations in Piecewise-Smooth Continuous Systems.*, volume 70 of *Nonlinear Science*. World Scientific, Singapore, 2010.

[169] D.J.W. Simpson. On the relative coexistence of fixed points and period-two solutions near border-collision bifurcations. *Appl. Math. Lett.*, 38:162–167, 2014.

[170] D.J.W. Simpson. Scaling laws for large numbers of coexisting attracting periodic solutions in the border-collision normal form. *Int. J. Bifurcation Chaos*, 24(9):1450118, 2014.

[171] D.J.W. Simpson. Sequences of periodic solutions and infinitely many coexisting attractors in the border-collision normal form. *Int. J. Bifurcation Chaos*, 24(6):1430018, 2014.

[172] D.J.W. Simpson and J.D. Meiss. Neimark-Sacker bifurcations in planar, piecewise-smooth, continuous maps. *SIAM J. Appl. Dyn. Sys.*, 7(3):795–824, 2008.

[173] D.J.W. Simpson and J.D. Meiss. Shrinking point bifurcations of resonance tongues for piecewise-smooth, continuous maps. *Nonlinearity*, 22(5):1123–1144, 2009.

[174] D.J.W. Simpson and J.D. Meiss. Simultaneous border-collision and period-doubling bifurcations. *Chaos*, 19(3):033146, 2009.

[175] D.J.W. Simpson and J.D. Meiss. Resonance near border-collision bifurcations in piecewise-smooth, continuous maps. *Nonlinearity*, 23(12):3091–3118, 2010.

[176] N.B. Slater. The distribution of the integers N for which $\{\theta N\} < \phi$. *Proc. Cambridge Philos. Soc.*, 46:525–534, 1950.

[177] N.B. Slater. Gaps and steps for the sequence $n\theta$ mod 1. *Proc. Cambridge Philos. Soc.*, 63:1115–1123, 1967.

[178] E.D. Sontag. *Mathematical Control Theory.* Springer-Verlag, New York, 1998.

[179] I. Sushko and L. Gardini. Center bifurcation for a two-dimensional piecewise linear map. In [158], pages 49-78.

[180] I. Sushko and L. Gardini. Center bifurcation for two-dimensional border-collision normal form. *Int. J. Bifurcation Chaos*, 18(4):1029–1050, 2008.

[181] I. Sushko and L. Gardini. Degenerate bifurcations and border collisions in piecewise smooth 1D and 2D maps. *Int. J. Bifurcation Chaos*, 20(7):2045–2070, 2010.

[182] I. Sushko, L. Gardini, and T. Puu. Tongues of periodicity in a family of two-dimensional discontinuous maps of real Möbius type. *Chaos Solitons Fractals*, 21:403–412, 2004.

[183] R. Szalai and H.M. Osinga. Invariant polygons in systems with grazing-sliding. *Chaos*, 18(2):023121, 2008.

[184] R. Szalai and H.M. Osinga. Arnol'd tongues arising from a grazing-sliding bifurcation. *SIAM J. Appl. Dyn. Sys.*, 8(4):1434–1461, 2009.

[185] S. Tang, J. Liang, Y. Xiao, and R.A. Cheke. Sliding bifurcations of Filippov two stage pest control models with economic thresholds. *SIAM J. Appl. Math.*, 72(4):1061–1080, 2012.

[186] P.H.E. Tiesinga. Precision and reliability of periodically and quasiperiodically driven integrate-and-fire neurons. *Phys. Rev. E*, 65(4):041913, 2002.

[187] H.L. Trentelman, A.A. Stoorvogel, and M. Hautus. *Control Theory for Linear Systems.* Springer-Verlag, New York, 2001.

[188] V.I. Utkin. *Sliding Modes in Control Optimization.* Springer-Verlag, New York, 1992.

[189] B. Van der Pol and M.J.O. Strutt. On the stability of the solutions of Mathieu's equation. *Phil. Mag.*, 5(27):18–38, 1928.

[190] P. Veerman. Symbolic dynamics and rotation numbers. *Phys. A*, 134:543–576, 1986.

[191] P. Veerman. Symbolic dynamics of order-preserving orbits. *Phys. D*, 29:191–201, 1987.

[192] T.L. Vincent and W.J. Grantham. *Nonlinear and Optimal Control Systems.* Wiley, New York, 1997.

[193] M. Wiercigroch and B. De Kraker, editors. *Applied Nonlinear Dynamics and Chaos of Mechanical Systems with Discontinuities.*, Singapore, 2000. World Scientific.

[194] S. Wiggins. *Introduction to Applied Nonlinear Dynamical Systems and Chaos.*, volume 2 of *Texts in Appl. Math.* Springer-Verlag, New York, 2003.

[195] R.L. Williams and D.A. Lawrence. *Linear State-Space Control Systems.* Wiley, Hoboken, NJ, 2007.

[196] M. Wojtkowski. A model problem with the coexistence of stochastic and integrable behaviour. *Commun. Math. Phys.*, 80:453–464, 1981.

[197] W.-M. Yang and B.-L. Hao. How the Arnol'd tongues become sausages in a piecewise linear circle map. *Comm. Theoret. Phys.*, 8:1–15, 1987.

[198] G. Yuan, S. Banerjee, E. Ott, and J.A. Yorke. Border-collision bifurcations in the buck converter. *IEEE Trans. Circuits Systems I Fund. Theory Appl.*, 45(7):707–716, 1998.

[199] X. Zhao and D.G. Schaeffer. Alternate pacing of border-collision period-doubling bifurcations. *Nonlinear Dyn.*, 50(3):733–742, 2007.

[200] X. Zhao, D.G. Schaeffer, C.M. Berger, W. Krassowska, and D.J. Gauthier. Cardiac alternans arising from an unfolded border-collision bifurcation. *J. Comput. Nonlinear Dyn.*, 3(4):041004, 2008.

[201] Z.T. Zhusubaliyev and E. Mosekilde. *Bifurcations and Chaos in Piecewise-Smooth Dynamical Systems.* World Scientific, Singapore, 2003.

[202] Z.T. Zhusubaliyev and E. Mosekilde. Torus birth bifurcations in a DC/DC convertor. *IEEE Trans. Circuits Systems I Fund. Theory Appl.*, 53(8):1839–1850, 2006.

[203] Z.T. Zhusubaliyev and E. Mosekilde. Direct transition from a stable equilibrium to quasiperiodicity in non-smooth systems. *Phys. Lett. A*, 372:2237–2246, 2008.

[204] Z.T. Zhusubaliyev and E. Mosekilde. Equilibrium-torus bifurcation in nonsmooth systems. *Phys. D*, 237:930–936, 2008.

[205] Z.T. Zhusubaliyev, E. Mosekilde, and S. Banerjee. Multiple-attractor bifurcations and quasiperiodicity in piecewise-smooth maps. *Int. J. Bifurcation Chaos*, 18(6):1775–1789, 2008.

[206] Z.T. Zhusubaliyev, E. Mosekilde, S. De, and S. Banerjee. Transitions from phase-locked dynamics to chaos in a piecewise-linear map. *Phys. Rev. E*, 77:026206, 2008.

[207] Z.T. Zhusubaliyev, E. Mosekilde, S. Maity, S. Mohanan, and S. Banerjee. Border collision route to quasiperiodicity: Numerical investigation and experimental confirmation. *Chaos*, 16(2):023122, 2006.

[208] Z.T. Zhusubaliyev, E. Soukhoterin, and E. Mosekilde. Quasiperiodicity and torus breakdown in a power electronic DC/DC converter. *Math. Comput. Simulation*, 73:364–377, 2007.

[209] Z.T. Zhusubaliyev, E.A. Soukhoterin, and E. Mosekilde. Border-collision bifurcations on a two-dimensional torus. *Chaos Solitons Fractals*, 13(9):1889–1915, 2002.

[210] Z.T. Zhusubaliyev, O.O. Yanochkina, E. Mosekilde, and S. Banerjee. Two-mode dynamics in pulse-modulated control systems. *Annual Rev. Control*, 34:62–70, 2010.